ARTICLE

Retromer has a selective function in cargo sorting via endosome transport carriers

Yi Cui[1], Julian M. Carosi[2,3]*, Zhe Yang[1]*, Nicholas Ariotti[4] iD, Markus C. Kerr[4] iD, Robert G. Parton[4] iD, Timothy J. Sargeant[2,5], and Rohan D. Teasdale[1] iD

Retromer is a peripheral membrane protein complex that coordinates multiple vesicular trafficking events within the endolysosomal system. Here, we demonstrate that retromer is required for the maintenance of normal lysosomal morphology and function. The knockout of retromer subunit Vps35 causes an ultrastructural alteration in lysosomal structure and aberrant lysosome function, leading to impaired autophagy. At the whole-cell level, knockout of retromer Vps35 subunit reduces lysosomal proteolytic capacity as a consequence of the improper processing of lysosomal hydrolases, which is dependent on the trafficking of the cation-independent mannose 6-phosphate receptor (CI-M6PR). Incorporation of CI-M6PR into endosome transport carriers via a retromer-dependent process is restricted to those tethered by GCC88 but not golgin-97 or golgin-245. Finally, we show that this retromer-dependent retrograde cargo trafficking pathway requires SNX3, but not other retromer-associated cargo binding proteins, such as SNX27 or SNX-BAR proteins. Therefore, retromer does contribute to the retrograde trafficking of CI-M6PR required for maturation of lysosomal hydrolases and lysosomal function.

Introduction

Lysosomes are dynamic organelles primarily associated with the degradation of macromolecules from the endocytic and autophagic pathway (Saftig and Klumperman, 2009; Settembre et al., 2013). The proteolytic activity of lysosomes requires the continuous delivery of newly synthesized acid hydrolases, which is achieved through multiple trafficking pathways. One of these is the mannose 6-phosphate receptor (M6PR)–dependent pathway, in which newly synthesized soluble acid hydrolase precursors acquire the mannose 6-phosphate sorting signal and are recognized by M6PR at the TGN (Saftig and Klumperman, 2009). Upon delivery to the endosome, the M6PR–hydrolase complexes dissociate owing to the acidic pH, and hydrolases are released to the lumen, whereas unoccupied M6PRs are retrieved to the TGN via the retrograde trafficking pathways. Defects in the M6PR trafficking itinerary lead to the inappropriate sorting and secretion of hydrolase precursors and, therefore, impair the degradative capacity of lysosomes (Ghosh et al., 2003).

The endosome-to-TGN retrieval of cargo molecules via endosome transport carriers (ETCs) is spatially and temporally coordinated by multiple protein regulators. One of these is retromer, a protein complex assembled from a high-affinity heterotrimeric core complex composed of Vps35, Vps29, and one of two Vps26

subunits, Vps26A or Vps26B (Kerr et al., 2005; Gokool et al., 2007; Hierro et al., 2007; Collins et al., 2008; Bugarcic et al., 2011). Retromer functions in exporting endosomal cargoes through molecular interactions with a range of associated proteins (Seaman, 2012). Several studies have shown that the retrograde transport of the cation-independent (CI)–M6PR relies on the coordination of retromer, and reduced levels of the retromer Vps35 or Vps26A subunits result in CI-M6PR mistrafficking (Arighi et al., 2004; Seaman, 2004, 2007, 2018; Wassmer et al., 2007; Bulankina et al., 2009; Kingston et al., 2011; McKenzie et al., 2012; McGough et al., 2014; Miura et al., 2014; Osborne et al., 2015; Tammineni et al., 2017; Hirst et al., 2018). Bugarcic et al. (2011) first observed that distinct subtypes of retromer, as defined by the Vps26 subunit incorporated, showed the distinct capacity to interact with and facilitate retrograde trafficking of CI-M6PR (Bugarcic et al., 2011). It is well established that numerous other non–retromer-associated proteins also contribute to the retrograde trafficking of CI-M6PR through direct or indirect mechanisms (Carlton et al., 2004; Wassmer et al., 2007; Hara et al., 2008; Breusegem and Seaman, 2014; Kvainickas et al., 2017; Simonetti et al., 2017). It remains controversial as to how many independent types of retrograde ETCs are formed from endosomes and what their relative

[1]School of Biomedical Sciences, Faculty of Medicine, The University of Queensland, Brisbane, Queensland, Australia; [2]Hopwood Centre for Neurobiology, Nutrition and Metabolism Theme, South Australian Health and Medical Research Institute, Adelaide, South Australia, Australia; [3]Centre for Cancer Biology, University of South Australia, Adelaide, South Australia, Australia; [4]Institute for Molecular Biosciences and Centre for Microscopy and Microanalysis, The University of Queensland, Brisbane, Queensland, Australia; [5]School of Pharmacy and Medical Sciences, University of South Australia, Adelaide, South Australia, Australia.

*J.M. Carosi and Z. Yang contributed equally to this paper; Correspondence to Rohan Teasdale: r.teasdale@uq.edu.au; N. Ariotti's present address is Mark Wainwright Analytical Centre, Electron Microscope Unit, The University of New South Wales, Sydney, New South Wales, Australia.

contribution to CI-M6PR trafficking is. Recent studies have even suggested that retromer does not contribute to this retrograde trafficking at all (Kvainickas et al., 2017; Simonetti et al., 2017).

Also required for the delivery of vesicles through the retrograde transport pathway are the TGN-located tethering proteins, which capture and direct the incoming cargo-loaded ETCs toward the TGN. A range of proteins including multi-subunit protein complexes and trans-Golgi–anchored long coiled-coil proteins have been shown to coordinate the tethering process (Bröcker et al., 2010; Munro, 2011). Recent studies reported that three GRIP domain–containing trans-golgins including GCC88, golgin-97, and golgin-245 are able to selectively capture a specific class of ETCs loaded with CI-M6PR and other retrograde cargoes (Wong and Munro, 2014). The vesicular tethering domains within golgin-97 and golgin-245 are closely related, whereas that in GCC88 is distinct, suggesting that trans-golgins capture different classes of ETCs (Gillingham and Munro, 2016).

In this study, we reveal that retromer is required for the maintenance of endolysosomal dynamics. Loss of retromer Vps35 subunit induces enlarged lysosomes at the ultrastructural level and leads to perturbations in autophagy and lysosomal proteolytic processes. The targeting and processing of M6PR-dependent hydrolases are impaired in the absence of retromer, which is consistent with CI-M6PR mistrafficking detected in retromer-depleted cells. Using the previously established mitochondria targeting assay (Wong and Munro, 2014), we further show that the retrograde sorting of CI-M6PR–loaded ETCs mediated by retromer is selectively tethered by GCC88, but not golgin-97 or golgin-245. This trafficking pathway requires SNX3-retromer association and is independent of the SNX27 or the SNX-BAR proteins.

Results

Ultrastructural alteration of lysosomal structures and elevated autophagy upon retromer deficiency

Aberrant lysosomal morphology and function were previously reported upon Vps35 knockdown in *Drosophila melanogaster* larva fat body cells (Maruzs et al., 2015). Using CRISPR/Cas9-mediated gene editing technology, clonal Vps35 knockout (KO) HeLa cells were generated, in which the core retromer subunit Vps35 was depleted, as determined by immunoblotting (Fig. 1 A). As expected, the absence of Vps35 prevents the formation of the trimeric retromer complex, resulting in reduced levels of the other two subunits, Vps26A and Vps29 (Fig. 1 A). Stable rescue cell lines were generated by the expression of GFP-tagged wild-type Vps35 in the Vps35 KO cell lines. By immunoblotting with Vps35, Vps26A, and Vps29 antibodies, we failed to detect any cell clones demonstrating full rescue of the expression for the retromer complex subunits (Fig. 1 A). Therefore, we selected the highest expressing clone for comparison. To determine whether the deficiency of retromer affects lysosomal compartments, we analyzed control HeLa cells and Vps35 KO cells using EM. Late endosomal/lysosomal structures, defined as large circular and electron-dense organelles, occupied ∼3% of the total cytoplasmic volume in the control HeLa cells (Fig. 1 B). In comparison, the lysosomes of Vps35 KO cells showed an almost threefold increase in volume (Fig. 1 B), which is similar to that described in *Drosophila*

models (Maruzs et al., 2015). Rescue of the Vps35 KO cells by expression of Vps35-GFP was able to fully restore this phenotype (Fig. 1 B). HeLa and Vps35 KO cells were next treated with LysoTracker Red, a fluorescent dye labeling acidic endolysosomal compartments. Flow cytometry revealed comparable levels of fluorescence intensities for LysoTracker-Red between HeLa and Vps35 KO cells (Fig. 1 C), which indicates similar levels of acidic endolysosomal compartments and further suggests that a proportion of the observed enlarged and electron-dense lysosomal compartments within Vps35 KO cells are not acidic and might represent lysosomes that are functionally impaired.

Functional lysosomes are required to fuse with autophagosomes for the final stages of autophagy. During this step, membrane bound LC3-II that exists on the luminal membrane of the autophagosome is degraded in the new autolysosomal environment. To determine whether retromer deficiency affects this process, the subcellular distribution of LC3-II was examined. HeLa, Vps35 KO, and Vps35-GFP rescue cells were coimmuno-labeled with antibodies against the endogenous LC3 and LAMP1, a late-endosome/lysosome marker. As indicated by confocal microscopy, Vps35 KO cells showed more membrane-bound LC3-II, with an increased colocalization with LAMP1, relative to HeLa and Vps35-GFP rescue cells (R_{HeLa} = 0.4983; $R_{Vps35\ KO}$ = 0.7217; $R_{Vps35-GFP\ rescue}$ = 0.3133; Fig. 1 D), suggesting reduced degradation of autophagic cargo caused by retromer deficiency. Changes in the basal levels of autophagy may be due to alterations in the kinetics of autophagy initiation (i.e., autophagosome formation) or the maturation of autophagosomes by fusion with lysosomes to generate functional degradation compartments, referred to as autophagic flux. These two processes can be uncoupled by chloroquine treatment, which selectively blocks the autophagic degradation function by preventing autophagosome-lysosome fusion (Mizushima et al., 2010). HeLa and Vps35 KO cells were treated with chloroquine for 6 h, and cell lysates were collected for immunoblotting. As expected, with chloroquine treatment, an increased level of LC3-II (approximately fivefold) was detected in HeLa cells (Fig. 1 E), consistent with a blockage of autophagic degradation. Vps35 KO cells exhibited higher basal levels of LC3-II (Fig. 1 E), which is in agreement with the immunofluorescent observations. Upon treatment with chloroquine, the LC3-II level increased slightly (∼1.5-fold) in Vps35 KO cells, which was still higher than that in treated HeLa cells (Fig. 1 E). These observations indicate that autophagosomes formed in Vps35 KO cells still undergo autophagic flux, which is inhibited by chloroquine treatment of these cells.

To further determine whether the induction of autophagy is affected by retromer deficiency, we investigated the intracellular activity of the mTORC1 signaling pathway, which is antagonistic to the induction of autophagy. As revealed by confocal microscopy, under amino acid–starved conditions, mTORC1 displayed a diffuse, cytoplasmic distribution in HeLa cells, whereas stimulation with essential amino acids promoted the recruitment of mTORC1 from the cytosol to lysosomal compartments, as demonstrated with colocalization with LAMP1 (Fig. 1 F). In Vps35 KO cells, although essential amino acid stimulation still resulted in the lysosomal recruitment of mTORC1, colocalization analysis indicated a significantly decreased recruitment compared with
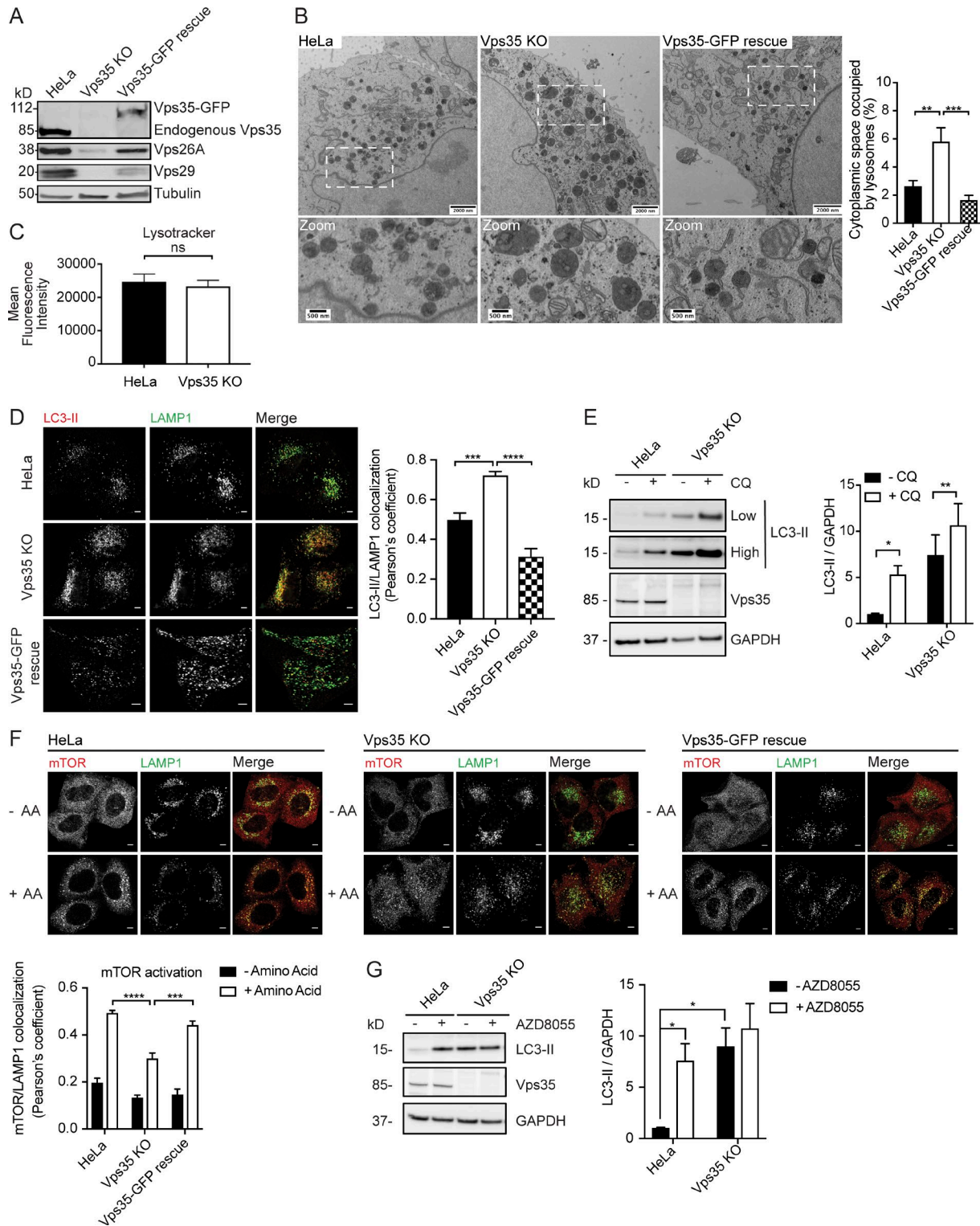
Figure 1. **Ultrastructural alteration of lysosomal structures and elevated autophagy in Vps35 KO cells. (A)** Generation of CRISPR/Cas9-mediated Vps35 KO HeLa cells and Vps35-GFP rescue cells. Equal amounts of cell lysates from HeLa, Vps35 KO, and Vps35-GFP rescue cells were subjected to SDS-PAGE and immunoblotted with antibodies against Vps35, Vps26A, Vps29, and tubulin. **(B)** Electron micrographs of HeLa, Vps35 KO, and Vps35-GFP rescue cells. Enlarged circular structures are indicated as late endosomal/lysosomal structures. Scale bars, 2,000 nm; in zoomed images, 500 nm. Graph represents the percentage volume density of lysosomal compartments relative to the cytoplasm in HeLa, Vps35 KO, and Vps35-GFP rescue cells (means ± SEM). Two-tailed Student's *t* test was used to determine the statistical significance. **, P < 0.01; ***, P < 0.001. *n* = two independent experiments with 10 images each. **(C)** Flow cytometric analysis of cellular acidification based on LysoTracker fluorescence in HeLa and Vps35 KO cells. Graph represents the mean fluorescent intensity within HeLa and Vps35 KO cells (means ± SEM). Two-tailed Student's *t* test was used to determine the statistical significance (*n* = 3). **(D)** HeLa, Vps35 KO, and Vps35-GFP rescue cells were fixed and coimmunolabeled with antibodies against LC3-II and LAMP1, followed by Alexa Fluor–conjugated fluorescent secondary antibodies. Scale bars, 5 µm. The colocalization between LC3-II and LAMP1 was quantified by the Pearson's correlation coefficient (means ± SEM). Two-tailed Student's *t*

HeLa control, suggesting decreased mTORC1 signaling activity. The decreased mTORC1 recruitment to lysosome by amino acid stimulation in Vps35 KO cells was rescued in Vps35-GFP rescue cells (HeLa: R_{-aa} = 0.1967, R_{+aa} = 0.4933; Vps35 KO: R_{-aa} = 0.1333, R_{+aa} = 0.3000; Vps35-GFP rescue: R_{-aa} = 0.1467, R_{+aa} = 0.4417; Fig. 1 F). To further confirm this finding, treatment of AZD8055, a pan-mTOR inhibitor, was used to examine the rate of autophagy initiation. HeLa and Vps35 KO cells were treated with AZD8055 for 25 h, and cell lysates were collected for immunoblotting. As expected, AZD8055-treated HeLa cells demonstrated increased LC3-II levels, consistent with an elevation in autophagy induction (Fig. 1 G). In contrast, mTORC1 inhibition in Vps35 KO cells did not increase the LC3-II level further compared with untreated cells, indicating little response in autophagy induction upon mTORC1 inhibition (Fig. 1 G). Taken together, these observations indicate that retromer deficiency induces dysfunctional autophagy by causing an elevated autophagy initiation and potentially altering the autophagic flux.

Retromer deficiency affects lysosomal activity

Because lysosomes play important roles in protein degradation, we compared intracellular proteolytic kinetics using DQ-BSA, a self-quenched dye conjugated with BSA, which enters into the endosomal system through endocytosis and generates a strong fluorescent signal upon proteolytic cleavage within lysosomal compartments. Initially, cells were treated with Alexa Fluor 647–conjugated BSA for 1 h at 37°C to measure the delivery efficiency of endocytosed material to endosomes. Fluorescence imaging showed no difference in fluorescent BSA conjugate staining between HeLa and Vps35 KO cells (Fig. 2 A), indicating comparable equilibrium rates of endocytosis/exocytosis for BSA trafficking. HeLa, Vps35 KO, and Vps35-GFP rescue cells were treated with DQ-BSA overnight, fixed, and immunolabeled with antibodies against the lysosome marker, LAMP1. Confocal microscopy and fluorescence intensity analysis revealed strong DQ-BSA fluorescence signal in both HeLa and Vps35-GFP rescue cell lines, which was largely overlapping with LAMP1 staining, indicating efficient proteolysis of DQ-BSA within lysosomes (Fig. 2 B). In contrast, Vps35 KO cells had a significantly lower DQ-BSA fluorescence within LAMP1-positive lysosomes, indicating impaired lysosomal proteolysis (Fig. 2 B).

Efficient lysosomal proteolysis is achieved through the action of various lysosomal enzymes. To determine whether lysosomal enzyme activities are affected by retromer deficiency, lysosomal subfractions from HeLa and Vps35 KO cells were purified and used to investigate the levels of four common enzymes β-hexosaminidase, acid phosphatase 2, β-galactosidase, and β-glucocerebrosidase. As indicated by immunoblotting, the mature forms of all four enzymes were detectable in lysosomal subfractions from control cells. In comparison, lysosomal subfractions from Vps35 KO cells demonstrated unchanged levels of β-glucocerebrosidase and acid phosphatase 2 (Fig. 2 C), both of which are targeted to lysosomes independent of M6PR (Markmann et al., 2015). β-Galactosidase and β-hexosaminidase depend on M6PR for delivery to lysosomes (Markmann et al., 2015), but only β-galactosidase displayed a moderate decrease in lysosome protein levels in Vps35 KO cells compared with HeLa control (Fig. 2 C). In addition, fluorometric analysis was used to examine the hydrolytic activity of the four enzymes in lysosomal subfractions from HeLa and Vps35 KO cells. In comparison to control cells, lysosomes purified from Vps35 KO cells demonstrated the same levels of enzyme activity for β-hexosaminidase, acid phosphatase, and β-glucocerebrosidase, but significantly reduced activity of β-galactosidase (Fig. 2 D), consistent with the observed protein levels. Collectively, these data suggest that the absence of retromer can selectively reduce the lysosomal targeting of M6PR-dependent enzymes, thereby affecting their functional levels within lysosomes. We next monitored the changes in enzyme targeting and activities within live intact cells using Magic Red cathepsin-B assay. HeLa and Vps35 KO cells were treated with Magic Red cathepsin-B, a cell-permeant fluorogenic substrate, which becomes fluorescent when cleaved by cathepsin enzymes in lysosomes. Live-cell time-lapse imaging and fluorescent intensity analysis revealed that Magic Red fluorescence in HeLa cells increased rapidly during the first 30 min, then maintained at relatively stable levels after that (Fig. 2 E). In contrast, fluorescence intensities for Magic Red in Vps35 KO cells were ∼40% lower than that in control cells, suggesting reduced cathepsin enzyme activity in the absence of retromer (Fig. 2 E). In contrast to other results, the Vps35-GFP rescue cells showed only a partial rescue of this phenotype, suggesting this aspect of endosome function is more sensitive to the level of retromer present in these cell models.

Retromer deficiency causes defects in CI-M6PR trafficking and its downstream cathepsin-D processing

Because the lysosomal activities of M6PR-dependent hydrolases were affected upon retromer KO, we next used cycloheximide chase experiments to investigate the processing and secretion of newly synthesized cathepsin-D, a well-characterized hydrolase relying on CI-M6PR for lysosomal delivery (Rojas et al., 2008; Bugarcic et al., 2011; Follett et al., 2014). HeLa and Vps35 KO cells

Figure 2. **Deficiency of retromer causes reduced lysosomal activity. (A)** HeLa and Vps35 KO cells were treated with AF647-conjugated BSA (200 µg/ml) in complete medium at 37°C for 1 h. Cells were then fixed and subjected to fluorescence microscopy. Graph represents the fluorescent intensity of endocytosed BSA conjugate within HeLa and Vps35 KO cells (means ± SEM). Two-tailed Student's t test was used to determine the statistical significance (n = 3). **(B)** HeLa, Vps35 KO, and Vps35-GFP rescue cells were treated with DQ-BSA Red (10 µg/ml) in complete medium at 37°C overnight. Cells were fixed and immunolabeled with antibodies against LAMP1, followed by Alexa Fluor–conjugated fluorescent secondary antibodies. Scale bars, 10 µm. Graph represents the fluorescent intensity of DQ-BSA Red within HeLa, Vps35 KO, and Vps35-GFP rescue cells (means ± SEM). Two-tailed Student's t test was used to determine the statistical significance (n = 3). *, P < 0.05; ***, P < 0.001. **(C)** Lysosomal subfractions from HeLa and Vps35 KO cells were prepared, and the protein levels of lysosome enzymes β-hexosaminidase, acid phosphatase 2, β-galactosidase, and β-glucocerebrosidase were determined by immunoblotting. Ponceau S staining of the relevant area of the blot was included as a loading control. Graph represents the level of β-galactosidase within the lysosome-enriched fraction of HeLa and Vps35 KO cells (means ± SEM). Two-tailed Student's t test was used to determine the statistical significance (n = 3). *, P < 0.05. **(D)** Lysosomal enzyme activities from lysosome-enriched fractions were analyzed by fluorometric analysis using a 4-MU detection system and were calculated in nmol · min⁻¹ · mg⁻¹ of input protein. Graph represents the fold difference of enzyme activities between HeLa and Vps35 KO cells (means ± SEM). Two-tailed Student's t test was used to determine the statistical significance (n = 3). *, P < 0.05. **(E)** HeLa, Vps35 KO, and Vps35-GFP rescue cells were treated with Magic Red Cathepsin-B in complete medium at 37°C and imaged by time-lapse video microscopy performed with the inverted Nikon Ti-E microscopy with Hamamatsu Flash 4.0 sCMOS camera. Graph represents the Magic Red Cathepsin B fluorescence intensity within HeLa, Vps35 KO, and Vps35-GFP rescue cells at the indicated time (means ± SEM). n = two independent experiments with eight random points each. *, P < 0.05; **, P < 0.01; ****, P < 0.0001.

were treated with cycloheximide, and medium samples were collected from cell monolayers containing equal number of cells at 0, 3, 6, and 9 h post-chase. As indicated by immunoblotting, the secreted cathepsin-D precursor was detected at 3 h post-chase in HeLa cells (Figs. 3 A and S1 A). In comparison, the secretion level of cathepsin-D precursor was significantly higher in the medium from Vps35 KO cells at 3 h post-chase, and further increased at 6 and 9 h post-chase (Figs. 3 A and S1 A). Immunoblotting of cell lysates to quantify tubulin levels confirmed that the secreted material was collected from equivalent numbers of cells (Fig. S1 A). Analysis of the cathepsin-D precursor in the untreated cell monolayer lysates indicates a higher level of precursor within Vps35 KO cells (Fig. S1, A and B). The ratio of secreted cathepsin-D precursor to the basal amount in the cell lysates showed that more than half of the precursor was secreted to the medium at 6 h post-chase in Vps35 KO cells, whereas only ~30% precursor was secreted in HeLa cells (Fig. S1 C). Collectively, these data indicate that retromer deficiency perturbs the intracellular processing of the cathepsin-D precursor, leading to its increased secretion rather than delivery to endosomes.

Impairment of M6PR-dependent lysosomal enzymes is most likely due to improper intracellular trafficking of CI-M6PR. Dysregulation of retromer has been previously shown to perturb the endosome-to-TGN delivery of CI-M6PR (Arighi et al., 2004; Seaman, 2004; Wassmer et al., 2007; Bugarcic et al., 2011; Kingston et al., 2011; McKenzie et al., 2012; Miura et al., 2014; Osborne et al., 2015; Tammineni et al., 2017; Hirst et al., 2018). To examine whether the retrograde transport of CI-M6PR is perturbed in the Vps35 KO cells, we performed a series of colocalization experiments using TGN and endosome markers. HeLa and Vps35 KO cells were coimmunolabeled with antibodies against endogenous CI-M6PR together with individual organelle markers. As expected, CI-M6PR was observed to tightly localize to perinuclear regions in control cells at steady state and displayed high levels of colocalization with p230-positive TGN, EEA1-positive early endosomes, and transferrin receptor (TfR)–positive recycling endosomes, but with minor or no overlap with LAMP1-positive lysosomes (Fig. 3 B). However, its intracellular distribution was clearly altered in Vps35 KO cells, displaying a relatively dispersed peripheral pattern (Fig. 3 B), in agreement with previously observations (Arighi et al., 2004; Seaman, 2004; Wassmer et al., 2007; Bugarcic et al., 2011; Kingston et al., 2011; McKenzie et al., 2012; Miura et al., 2014; Osborne et al., 2015; Tammineni et al., 2017; Hirst et al., 2018). In fact, colocalization analysis revealed a reduced overlap of CI-M6PR with p230, but a mildly increased overlap with EEA1 and TfR in Vps35 KO cells (p230: R_{HeLa} = 0.4005, $R_{Vps35 KO}$ = 0.3264; EEA1: R_{HeLa} = 0.4220, $R_{Vps35 KO}$ = 0.5219; TfR: R_{HeLa} = 0.4229, $R_{Vps35 KO}$ = 0.5007; Fig. 3 B), suggesting impaired CI-M6PR retrograde transport in the absence of retromer. To further confirm the disrupted trafficking itinerary caused by retromer deficiency, we next used a CD8α internalization assay to investigate the intracellular trafficking of CI-M6PR. HeLa and Vps35 KO cells transiently transfected with the CD8α-CI-M6PR reporter were incubated with antibodies against CD8α on ice for 30 min and washed twice with acid solutions. CD8α internalization was then chased at 37°C for up to 60 min, fixed, and immunolabeled with antibodies against

golgin-97, a TGN marker, or Rab5, an early endosome marker. As revealed by confocal microscopy and colocalization analysis, antibodies bound to CD8α-CI-M6PR were internalized following endocytic pathways and delivered to the golgin-97 positive TGN compartment at 60 min post-chase in control cells, suggesting the efficient retrograde transport of the reporter (Fig. 3 C). In contrast, reduced CD8α-CI-M6PR delivery to the TGN was observed in Vps35 KO cells, which was correlated with a significantly increased colocalization with early endosomal compartments at 60 min post-chase (Golgin-97: R_{HeLa} = 0.3908, $R_{Vps35 KO}$ = 0.2340; Rab5: R_{HeLa} = 0.1960, $R_{Vps35 KO}$ = 0.2453; Fig. 3 C). These data indicate that retromer is required for the efficient retrograde transport of CI-M6PR, and its deficiency induces increased receptor retained in endosomal compartments.

A subset of CI-M6PR–containing endosome-derived transport vesicles that are tethered by GCC88 depend on retromer for their generation

Retrograde transport of CI-M6PR is achieved by multiple intracellular pathways engaging a range of intracellular machinery. For example, GRIP domain–containing golgin proteins including GCC88, golgin-97, and golgin-245 have all been implicated as the tethering proteins for ETCs incorporating CI-M6PR (Lieu et al., 2007; Wong and Munro, 2014). We have applied a recently developed rerouting and capture assay, by which mitochondrial targeted golgins capture and relocate ETCs loaded with specific classes of cargoes to the mitochondria instead of the TGN (Wong and Munro, 2014). HeLa and Vps35 KO cells were transiently transfected with individual HA-tagged golgin-MAO constructs, in which the golgin's C-terminal Golgi-targeting domain was engineered to be replaced by the mitochondria-targeting transmembrane domain of monoamine oxidase (MAO; Wong and Munro, 2014). Transfected cells were fixed and coimmunolabeled against HA and endogenous CI-M6PR. Confocal microscopy revealed a filamentous, mitochondrial pattern for CI-M6PR in control cells when expressing GCC88-MAO, golgin-97-MAO, or golgin-245-MAO construct, whereas cells expressing the cis-golgin, GM130-MAO, demonstrated little relocation of CI-M6PR to the mitochondria (Fig. 4 A), consistent with previous observations (Wong and Munro, 2014). Indeed, colocalization analysis indicated significant overlap of CI-M6PR with HA-labeled golgin-MAO in HeLa cells expressing GCC88-MAO, golgin-97-MAO, or golgin-245-MAO (HeLa: $R_{GCC88-MAO}$ = 0.3911, $R_{golgin-97-MAO}$ = 0.6186, and $R_{golgin-245-MAO}$ = 0.3564), compared with that of cells expressing GM130-MAO (HeLa: $R_{GM130-MAO}$ = 0.1516; Fig. 4 B). Retromer deficiency did not affect the relocation of CI-M6PR–loaded ETCs captured by golgin-97-MAO and golgin-245-MAO, but it did perturb the relocation of CI-M6PR ETCs tethered by GCC88 (Fig. 4 A). In support of this, colocalization analysis revealed a high level of overlap of CI-M6PR with golgin-97-MAO or golgin-245-MAO in Vps35 KO cells (Vps35 KO: $R_{golgin-97-MAO}$ = 0.5890 and $R_{golgin-245-MAO}$ = 0.2906), which was similar to control HeLa, but a significant reduction in the colocalization of CI-M6PR with GCC88-MAO (Vps35 KO: $R_{GCC88-MAO}$ = 0.1772; Fig. 4 B). Taken together, these data indicate that retromer is selectively required for the incorporation of CI-M6PR into a subset of ETCs defined by their capacity to be tethered by GCC88. To determine
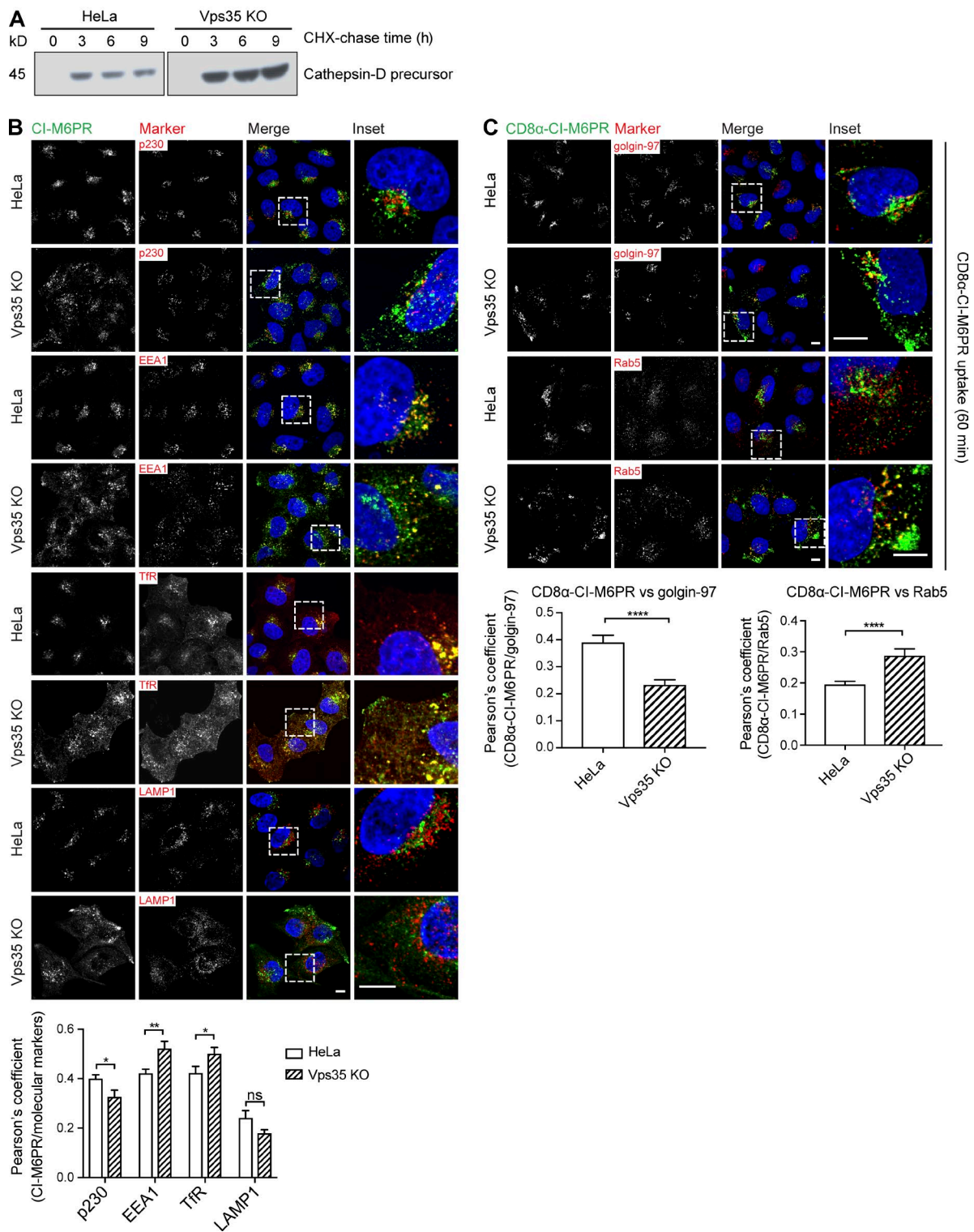
Figure 3. **Vps35 is required for efficient CI-M6PR trafficking and cathepsin-D processing. (A)** HeLa and Vps35 KO cells were pulsed with 100 µg/ml cyclohex-imide in serum-free medium containing 2 mM glutamine for 0, 3, 6, and 9 h. The medium samples were collected from cell monolayers containing equal numbers of cells and subjected to immunoblotting with antibodies against cathepsin-D. **(B)** The distribution of CI-M6PR in HeLa and Vps35 KO cells was determined by indirect immunofluorescence using antibodies against endogenous CI-M6PR, p230, EEA1, TfR, and LAMP1. Scale bars, 10 µm. The colocalization between CI-M6PR and different organelle markers was quantified by the Pearson's correlation coefficient and represented in graphs (means ± SEM). Two-tailed Student's *t* test was used to determine the statistical significance (*n* = 3). *, P < 0.05; **, P < 0.01. **(C)** The internalization assay was performed in HeLa and Vps35 KO cells transiently transfected with the CD8α-CI-M6PR construct, using antibodies against CD8α. The delivery of CD8α-CI-M6PR complex to the TGN and early endosome after uptake for 60 min at 37°C was determined by indirect immunofluorescence using antibodies against golgin-97 and Rab5, followed by Alexa Fluor–conjugated fluorescent secondary antibodies. Scale bars, 10 µm. The colocalization between CD8α-CI-M6PR and indicated molecular markers was quantified by the Pearson's correlation coefficient and represented in graphs (means ± SEM). Two-tailed Student's *t* test was used to determine the statistical significance (*n* = 3). ****, P < 0.0001.

whether retromer can be retained on the released ETCs and potentially function as part of the GCC88 tethers, confocal microscopy and colocalization analysis revealed little overlap of Vps35 with GCC88-MAO or the other mitochondrial targeted golgins (Fig. S2 A), suggesting that retromer is not associated with the ETCs released from the endosomes, which is consistent with previous reports (Arlt et al., 2015).

To further test the specificity for GCC88-tethered retromer-sorted ETCs, we performed the rerouting assay to investigate the trafficking of cation-dependent (CD)–M6PR, proposed to be a retromer-independent retrograde cargo (Arighi et al., 2004; Seaman, 2004). HeLa and Vps35 KO cells were transiently transfected with individual HA-tagged golgin-MAO constructs, fixed, and immunolabeled with antibodies against HA and endogenous CD-M6PR. Confocal microscopy revealed relocation of CD-M6PR–loaded ETCs to the mitochondria in both control HeLa and Vps35 KO cells transfected with the GCC88-MAO, golgin-97-MAO, or golgin-245-MAO construct (Fig. 4 C and Fig. S3). This observation was further supported by the colocalization analysis (HeLa: $R_{GCC88-MAO}$ = 0.3973, $R_{golgin-97-MAO}$ = 0.6798, $R_{golgin-245-MAO}$ = 0.5045, and $R_{GM130-MAO}$ = 0.1183; Vps35 KO: $R_{GCC88-MAO}$ = 0.2783, $R_{golgin-97-MAO}$ = 0.7056, $R_{golgin-245-MAO}$ = 0.5537, and $R_{GM130-MAO}$ = 0.0796; Fig. 4 C). Collectively, these data suggest that the absence of retromer has no impact on GCC88-captured ETCs loaded with cargoes that traffic in a retromer-independent manner. These observations are consistent with retromer functions involving a direct action in ETC formation and protein trafficking, through binding with its associated cargoes, including CI-M6PR.

To confirm this phenotype, two additional cell models were generated. First, a stable WT Vps35 rescue cell line was generated by the expression of untagged WT Vps35 in the Vps35 KO cell lines (Fig. S2 B). Second, a second retromer subunit, Vps26A KO cell line, was independently generated using the same approach. These cell lines were used for the rerouting assay to investigate the trafficking of CI-M6PR vesicles (Figs. 4 D and S2 B). Vps35 KO, Vps35-GFP rescue, Vps35-wt rescue, and Vps26A KO cells were transiently transfected with GCC88-MAO or GM130-MAO, fixed, and coimmunolabeled with antibodies against HA and endogenous CI-M6PR. As expected, CI-M6PR staining in both Vps35 rescue cell lines showed a significantly increased colocalization with HA-GCC88-MAO compared with Vps35 KO cell line (Vps35-GFP rescue: $R_{GCC88-MAO}$ = 0.4363; Vps35-wt rescue: $R_{GCC88-MAO}$ = 0.3634; Vps35 KO: $R_{GCC88-MAO}$ = 0.1548; Fig. 4 D). The Vps26A KO cells showed the same phenotype as the Vps35 KO cells with a reduced colocalization of CI-M6PR with HA-GCC88-MAO, compared with control cells (HeLa: $R_{GCC88-MAO}$ = 0.4258; Vps26A KO: $R_{GCC88-MAO}$ = 0.1789; Fig. S2 C). These results further verify the essential action of retromer in the retrograde transport of GCC88-tethered CI-M6PR vesicles.

SNX3 associates with retromer to coordinate the trafficking of GCC88-tethered CI-M6PR–containing ETC

Current models propose that within endosomes, the retromer contributes to the sorting and transport of a range of cargoes via interactions with distinct cargo-binding proteins. To determine which of these are contributing to retromer-dependent trafficking of CI-M6PR, we generated a series of KO cells depleted

for the following cargo binding retromer complexes: SNX3-Retromer, SNX-BAR-Retromer, and SNX27-Retromer. Initially, we used the CRISPR/Cas9-based targeting plasmids to generate clonal SNX1/2 double knockout (dKO), SNX3 KO, and SNX27 KO cell lines. HeLa SNX27 KO was generated as described previously (Clairfeuille et al., 2016). Immunoblotting revealed the absence of SNX1 and SNX2 in SNX1/2 dKO cell line (Fig. 5 A), further resulting in the loss of SNX5 and SNX6 expression, whose stability and endosome recruitment is dependent on the formation of the functional SNX-BAR dimers (Kerr et al., 2006). On the other hand, the depletion of SNX1/2, SNX3, or SNX27 had no effect on the levels of Vps35 and Vps26A (Fig. 5 A). The rerouting assay was then performed using these KO cell lines to investigate the trafficking of GCC88-tethered CI-M6PR vesicles. HeLa, SNX1/2 dKO, SNX3 KO, and SNX27 KO cells were transiently transfected with HA-tagged GCC88-MAO or GM130-MAO, fixed, and coimmunolabeled with antibodies against HA and endogenous CI-M6PR. Colocalization analysis was performed to quantify the relocation of CI-M6PR to the golgin-positive mitochondria. CI-M6PR is redistributed to the mitochondria in GCC88-MAO–transfected HeLa cells (HeLa: $R_{GCC88-MAO}$ = 0.3804; Figs. 5 B and S4 A). Similar levels of overlap between CI-M6PR and GCC88-MAO were observed in both SNX1/2 dKO cells and SNX27 KO cells, compared with the control cells (SNX1/2 dKO: $R_{GCC88-MAO}$ = 0.4340; SNX27 KO: $R_{GCC88-MAO}$ = 0.3950; Figs. 5 B and S4 A). In contrast, a significantly decreased colocalization of CI-M6PR with GCC88-MAO was detected in SNX3 KO cells (SNX3 KO: $R_{GCC88-MAO}$ = 0.1556; Figs. 5 B and S4 A), which was similar to that observed in Vps35 KO cells. These data indicate that apart from the retromer, the endosomal transport of the subset of CI-M6PR vesicles captured by GCC88 also depends on the coordination of SNX3, but not SNX-BAR proteins and SNX27. Like retromer, SNX3 was not redistributed to the mitochondria in HeLa cells expressing GCC88-MAO, indicating it is not associated with these mature ETCs which are recognized and tethered by GCC88 (Fig. S2 C). The possibility that SNX proteins might directly coordinate CI-M6PR retrieval independent of retromer has been recently suggested (Elwell et al., 2017; Kvainickas et al., 2017; Simonetti et al., 2017). Given this, we further examined the trafficking of CI-M6PR ETCs tethered by golgin-97 or golgin-245 in SNX KO cell lines. As indicated by confocal microscopy and colocalization analysis, SNX1/2 dKO, SNX3 KO, and SNX27 KO cells all showed comparable levels of colocalization between CI-M6PR and golgin-97-MAO, compared with the HeLa control cells (HeLa: $R_{golgin-97-MAO}$ = 0.7330; SNX1/2 dKO: $R_{golgin-97-MAO}$ = 0.7562; SNX3 KO: $R_{golgin-97-MAO}$ = 0.7431; SNX27 KO: $R_{golgin-97-MAO}$ = 0.7323; Figs. 5 B and S4 B). In contrast, SNX1/2 dKO cells demonstrated a decreased colocalization level between CI-M6PR and golgin-245-MAO, whereas SNX3 KO and SNX27 KO cells remained at a similar colocalization level with HeLa cells (HeLa: $R_{golgin-245-MAO}$ = 0.4796; SNX1/2 dKO: $R_{golgin-245-MAO}$ = 0.2580; SNX3 KO: $R_{golgin-245-MAO}$ = 0.5747; SNX27 KO: $R_{golgin-245-MAO}$ = 0.4660; Figs. 5 B and S4 C), indicating that SNX-BAR proteins contribute to the trafficking of the subset of CI-M6PR ETCs that are captured by golgin-245.

We next examined the transport of CD-M6PR, a retromer-independent cargo, in the SNX KO cell lines, through the rerouting assay. As indicated by the colocalization analysis, SNX1/2
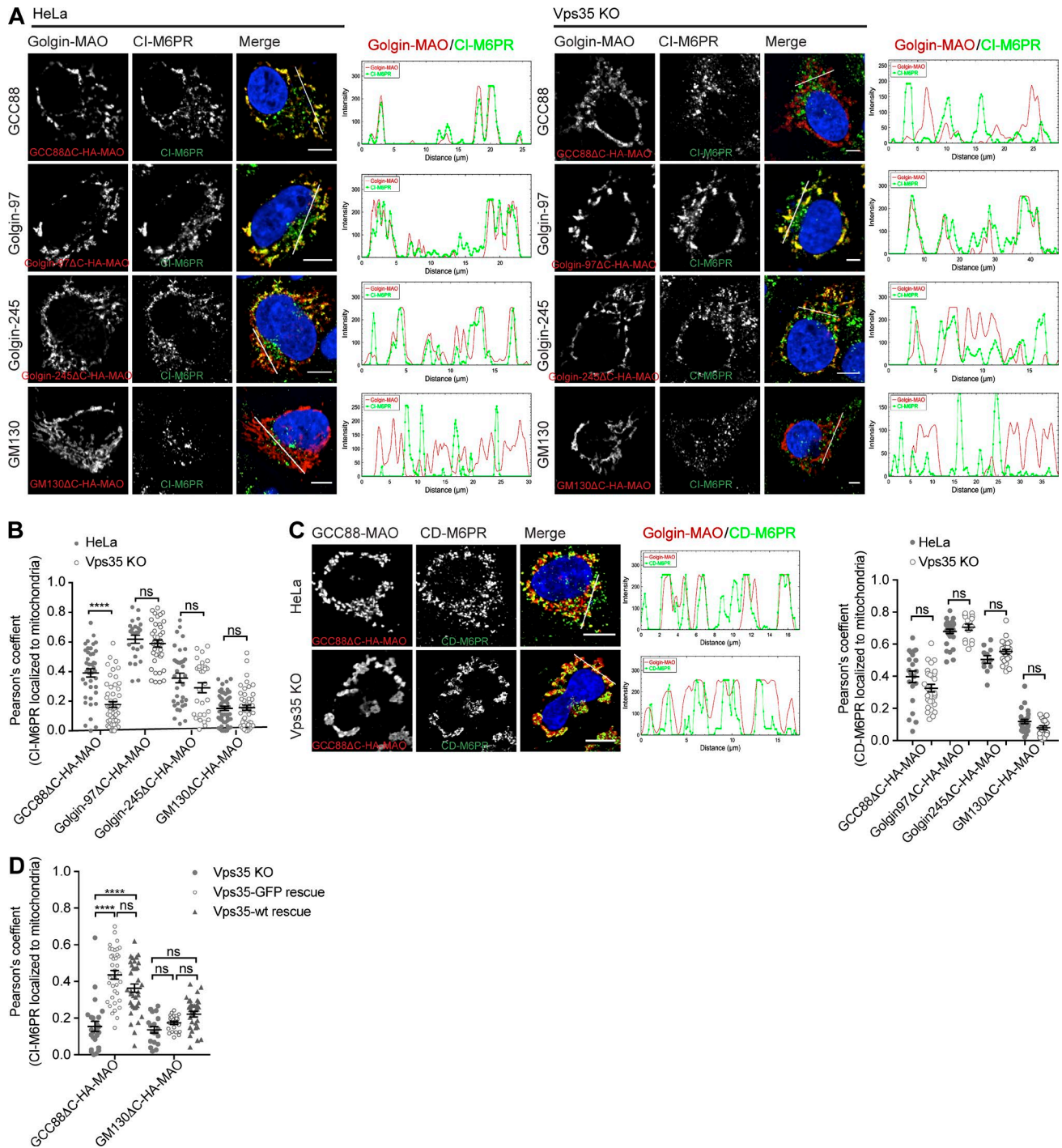
Figure 4. **ETCs containing CI-M6PR, which are tethered by GCC88, are absent in Vps35 KO cells. (A)** HeLa and Vps35 KO cells were transiently transfected with individual HA-tagged mitochondria-targeting golgin constructs: GCC88-MAO, Golgin-97-MAO, Golgin-245-MAO, and GM130-MAO. Cells were fixed and coimmunolabeled with antibodies against HA and endogenous CI-M6PR, followed by Alexa Fluor–conjugated fluorescence secondary antibodies. Scale bars, 10 µm. The intensity plots of the fluorescent intensity (y-axis) against distance (x-axis) represent the overlap between channels. **(B)** The colocalization between CI-M6PR and HA-tagged golgin-mito proteins was quantified by Pearson's correlation coefficient (means ± SEM). Two-tailed Student's t test was used to determine the statistical significance (n = 3). ****, P < 0.0001. **(C)** HeLa and Vps35 KO cells were transiently transfected with HA-tagged mitochondria-targeting golgin constructs GCC88-MAO, Golgin-97-MAO, Golgin-245-MAO, and GM130-MAO; fixed; and coimmunolabeled with antibodies against HA and endogenous CD-M6PR, followed by Alexa Fluor–conjugated fluorescence secondary antibodies. Scale bars, 10 µm. The intensity plots of the fluorescent intensity (y-axis) against distance (x-axis) represent the overlap between channels. The colocalization between CD-M6PR and HA-tagged golgin-mito proteins was quantified by Pearson's correlation coefficient (means ± SEM). Two-tailed Student's t was used to determine the statistical significance (n = 3). **(D)** Vps35 KO, Vps35-GFP rescue, and the untagged wild-type Vps35 rescue cells were transiently transfected with HA-tagged GCC88-MAO or GM130-MAO construct, fixed, and coimmunolabeled with antibodies against HA and endogenous CI-M6PR, followed by Alexa Fluor–conjugated fluorescence secondary antibodies. The colocalization between CI-M6PR and HA-tagged golgin-mito protein GCC88 and GM130 was quantified by Pearson's correlation coefficient (means ± SEM). Two-tailed Student's t test was used to determine the statistical significance (n = 3). ****, P < 0.0001.
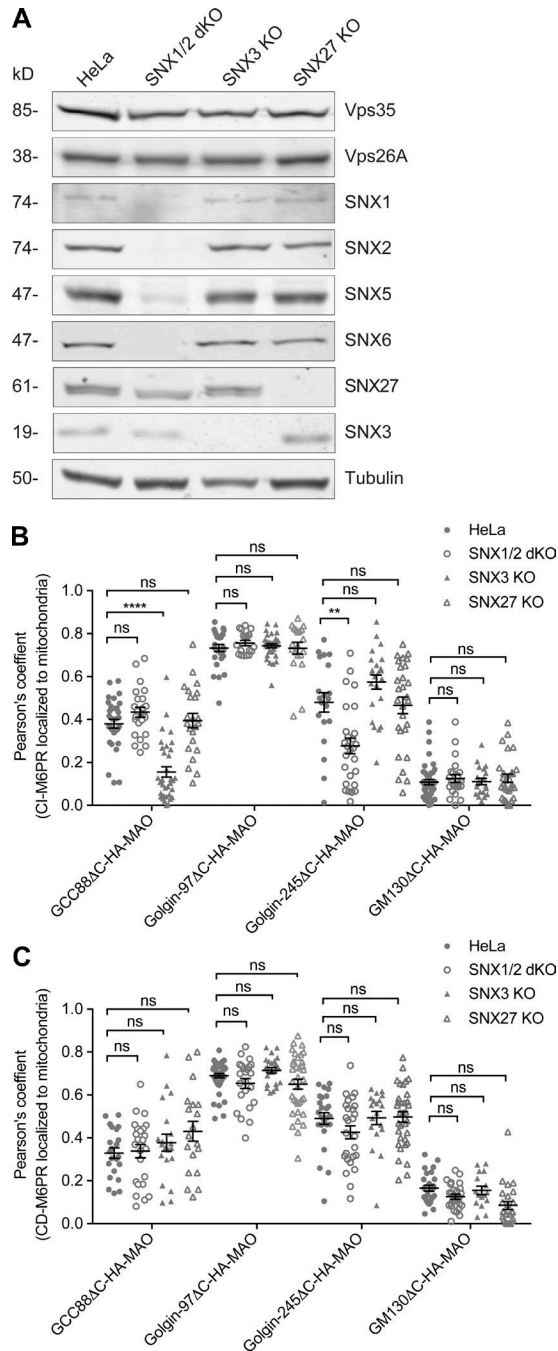
Figure 5. **SNX3 is required for the retrograde transport of CI-M6PR GCC88-tethered ETCs. (A)** Equal amounts of cell lysates from HeLa, SNX1/2 dKO, SNX3 KO, and SNX27 KO cells were subjected to SDS-PAGE and immunoblotted with antibodies against Vps35, Vps26A, SNX1, SNX2, SNX5, SNX6, SNX27, SNX3, and tubulin. **(B and C)** HeLa, SNX3 KO, SNX1/2 dKO, and SNX27 cells were transiently transfected with HA-tagged mitochondria-targeting golgin constructs GCC88-MAO, Golgin-97-MAO, Golgin-245-MAO, or GM130-MAO; fixed; and coimmunolabeled with antibodies against HA and endogenous CI-M6PR (B) or CD-M6PR (C), followed by Alexa Fluor–conjugated secondary antibodies. The intensity plots of the fluorescent intensity (y-axis) against distance (x-axis) represent the overlap between channels. The colocalization of CI-M6PR (B) or CD-M6PR (C) with HA-tagged golgin-mito proteins was quantified by Pearson's correlation coefficient (means ± SEM). Two-tailed Student's t test was used to determine the statistical significance (n = 3). **, $P < 0.01$; ****, $P < 0.0001$.

dKO, SNX3 KO, and SNX27 KO cells all demonstrated considerable overlap of CD-M6PR with GCC88-MAO that was similar to control cells (HeLa: $R_{GCC88-MAO}$ = 0.3285; SNX1/2 dKO: $R_{GCC88-MAO}$ = 0.3383; SNX3 KO: $R_{GCC88-MAO}$ = 0.3530; SNX27 KO: $R_{GCC88-MAO}$ = 0.4306; Figs. 5 C and S5 A). In addition, the redirection of CD-M6PR ETCs captured by golgin-97 or golgin-245 was not affected in SNX3 KO and SNX27 KO cells, as well as in SNX1/2 dKO cells (HeLa: $R_{golgin-97-MAO}$ = 0.6899 and $R_{golgin-245-MAO}$ = 0.4899; SNX1/2 dKO: $R_{golgin-97-MAO}$ = 0.6536 and $R_{golgin-245-MAO}$ = 0.4262; SNX3 KO: $R_{golgin-97-MAO}$ = 0.7145 and $R_{golgin-245-MAO}$ = 0.4928; SNX27 KO: $R_{golgin-97-MAO}$ = 0.6505 and $R_{golgin-245-MAO}$ = 0.4973; Figs. 5 C and S5, B and C). Therefore, these data suggest that the absence of SNX3, SNX1/2, and SNX27 has no essential role in the protein trafficking of CD-M6PR within ETCs captured by GCC88, golgin-97, or golgin-245.

Discussion

The endolysosomal system represents a dynamic set of intracellular compartments that play a critical role in the protein trafficking and degradation of transmembrane and soluble cargoes within the cell. The maintenance of endolysosomal homeostasis is achieved via the temporally and spatially coordination of multiple protein machineries. Enlarged lysosomal structures were observed in the absence of Vps35, which is consistent with previous reports in retromer-depleted *Drosophila* photoreceptor cells and larva fat body cells (Wang et al., 2014; Maruzs et al., 2015), as well as mammalian cells (Arighi et al., 2004). We propose that the enlarged lysosomal structures observed in the absence of Vps35 are caused by the improper trafficking of newly synthesized lysosomal enzymes by CI-M6PR, which decreases the lysosomal degradative activities and therefore results in an accumulation of undegraded materials within lysosomal compartments. It remains to be determined whether the absence of retromer directly affects the recently observed lysosome maturation cycle (Bright et al., 2016). Changes of lysosomal functions upon depletion of Vps35 are in agreement with the roles of lysosome in the regulation of autophagy and other signaling cascades. The levels of LC3-II, an adaptor and cargo for the autophagosome, were greatly increased upon the depletion of Vps35. This is partially due to the decreased lysosomal proteolytic activity but also reflected by the contribution of the interaction between retromer and TBC1D5 in the controlling of LC3 shuttling (Roy et al., 2017). Lysosomal compartments, in contrast, appear to act as a central scaffold in the lysosomal recruitment of mTORC1 and the subsequent mTORC1 activation through various mechanisms (Goberdhan et al., 2016). Consistent with this concept, mTORC1 recruitment to the lysosome in response to amino acid stimulation in Vps35 KO cells was greatly diminished, indicating that impaired lysosomal function impairs mTORC1 recruitment and activation.

Since being initially identified (Arighi et al., 2004; Seaman, 2004), retromer has been considered to function in the coordination of the endosomal protein sorting and trafficking of a variety of cargo molecules. It is well established that the endosome-to-TGN retrieval of CI-M6PR is mediated by retromer. Previous studies demonstrate an impaired trafficking itinerary of CI-M6PR upon the depletion of Vps35 (Wassmer et al.,

2007; Miura et al., 2014; Osborne et al., 2015; Hirst et al., 2018) or Vps26A (Arighi et al., 2004; Seaman, 2004; Wassmer et al., 2007; McKenzie et al., 2012) in mammalian cells, indicating a requirement for the retromer in the retrograde pathway. Our observations reconfirm the functional role of the retromer in the endosome-to-TGN retrieval of CI-M6PR. In cells with a complete knockout of Vps35, we observed a redistribution of CI-M6PR from the TGN to peripheral endosomal structures, causing defective lysosomal targeting and processing of CI-M6PR–dependent enzymes such as cathepsin-D and β-galactosidase. Intriguingly, we found that only a subset of CI-M6PR–containing ETCs sorted from endosomes to the TGN depend on retromer. Using the recently developed rerouting assay, which enables dissection of retrograde ETCs (Wong and Munro, 2014), we showed that the absence of Vps35 impairs the transport only of CI-M6PR ETCs that are captured by the trans-Golgi–anchored tethering factor GCC88, rather than other tethering factors such as golgin-97 or golgin-245. Our observations suggest a more limited but defined role of retromer in the CI-M6PR retrograde transport to the TGN, in support of the hypothesis that multiple types of machinery are involved in this retrograde trafficking (Díaz and Pfeffer, 1998; Meyer et al., 2000; Saint-Pol et al., 2004; Scott et al., 2006). This is consistent with the observation that Vps26B-containing retromer does not coprecipitate CI-M6PR (Bugarcic et al., 2011), which indicates that not all retromer complexes engage with the CI-M6PR. Likewise, a range of other endosome-associated proteins, including many associated with retromer, have been implicated in CI-M6PR retrograde trafficking. We observed that the CI-M6PR protein levels at the steady state were unchanged in the absence of Vps35 (unpublished data), consistent with other studies using the Vps35-depleted cells (Osborne et al., 2015; Hirst et al., 2018), indicating that retromer-independent retrograde trafficking of CI-M6PR still occurs. Recently, retromer having any role in the CI-M6PR retrograde trafficking has been questioned, based on observations that CI-M6PR was not redistributed in retromer KO cell lines (Kvainickas et al., 2017; Simonetti et al., 2017) and that its trafficking was dependent only on SNX-BAR proteins. With respect to retromer, the observations in these studies directly conflict with the data presented in this paper. Likewise, these studies conflict with the researchers' own earlier work in which efficient RNAi depletion identified that SNX5 and SNX6 alter CI-M6PR trafficking in the same way that suppression of known retromer subunits did (Wassmer et al., 2007). This difference with what we presume involves a consistent methodology was not discussed in their recent publications (Kvainickas et al., 2017; Simonetti et al., 2017). One explanation for the failure to observe a difference in CI-M6PR trafficking is that both studies (Kvainickas et al., 2017; Simonetti et al., 2017) determined changes in CI-M6PR trafficking based on correlation/colocalization relative to TGN46 only. Before these studies, it was already well established that TGN46 is incorporated in the ETCs (Wong and Munro, 2014) and that its retrograde trafficking was dependent on retromer (Lieu and Gleeson, 2010) and SNX-BAR proteins (Wassmer et al., 2007). Therefore, both CI-M6PR and TGN46 would be expected to change cellular distribution in the absence of the retromer. Furthermore, these studies with respect to retromer would be considered incomplete, as neither

includes the standard assay used for CI-M6PR trafficking which is the mistrafficking of newly synthesized lysosomal hydrolases.

We also demonstrated that the retrograde transport of CI-M6PR through ETCs tethered by GCC88 was perturbed in the absence of SNX3. This observation is consistent with previous reports that RNAi knockdown of SNX3 alters CI-M6PR retrograde transport (Harbour et al., 2010; Priya et al., 2017). SNX3 interacts with the retromer subunits Vps35 and Vps26 via multiple interfaces through its N-terminal tail, and this molecular interaction enables the endosomal recruitment of retromer via the SNX3 PX domain (Harterink et al., 2011; Vardarajan et al., 2012; Harrison et al., 2014; Lucas et al., 2016; Lenoir et al., 2018). Recent structural studies determined that at the interface between Vps26 and SNX3, there is a binding site for a canonical sorting signal, ØX(L/M) consensus motif (where Ø can be any hydrophobic amino acid) for cargo recognition by retromer (Tabuchi et al., 2010; Lucas et al., 2016). The recycling motif of the divalent metal transporter 1 isoform II (DMT1-II), a retromer cargo that cycles between the endosome to the cell surface, has been shown to fit in this binding mode, demonstrating the role of SNX3-retromer interaction in cargo sorting and membrane recruitment (Lucas et al., 2016). CI-M6PR has a related sorting motif with the structural properties that would enable it to interact with SNX3-retromer (Seaman, 2007; Lucas et al., 2016), which supports this as the molecular mechanism by which SNX3 contributes to retromer-dependent CI-M6PR retrograde transport.

Apart from SNX3, we also examined other cargo-binding retromer associated proteins including SNX-BAR and SNX27. Intriguingly, our data demonstrate that the dKO of SNX-BAR proteins, SNX1 and SNX2, which results in the endosomal dissociation of SNX5 and SNX6, has no impact on the intracellular trafficking of GCC88-tethered CI-M6PR vesicles, suggesting that the SNX-BAR dimer is not required for this endosomal sorting process. We did observe, however, that the trafficking of golgin-245–tethered CI-M6PR vesicles was affected in SNX1/2 dKO cells, raising the possibility that the SNX-BAR dimer may function independently of retromer in the retrograde transport of CI-M6PR vesicles. These observations are consistent with previous reports demonstrating that the deficiency of SNX-BAR dimer alters CI-M6PR retrieval (Carlton et al., 2004; Wassmer et al., 2007; Hara et al., 2008; Hong et al., 2009) and are supported by recent studies suggesting the direct interaction between SNX5 and CI-M6PR (Elwell et al., 2017; Kvainickas et al., 2017; Simonetti et al., 2017). It has been identified that golgin-97 and golgin-245 capture ETCs that are decorated with the WASH complex through a vesicle-golgin adaptor protein TBC1D23 (Shin et al., 2017). Given the established association between the WASH complex and retromer (Gomez and Billadeau, 2009; Harbour et al., 2012; Jia et al., 2012), it is difficult to reconcile why the knockout of retromer does not disrupt the trafficking of CI-M6PR vesicles captured by golgin-97 and golgin-245. However, as proposed by Shin et al. (2017), it is plausible that a redundant tethering mechanism is acting in parallel that may not be dissected by our experimental approaches (Shin et al., 2017). Recent reported proteomics data indicate that SNX27, another retromer accessory protein that functions in the recycling of cargo from endosomes to the plasma membrane, also associates with the CI-M6PR (Kvainickas et al.,
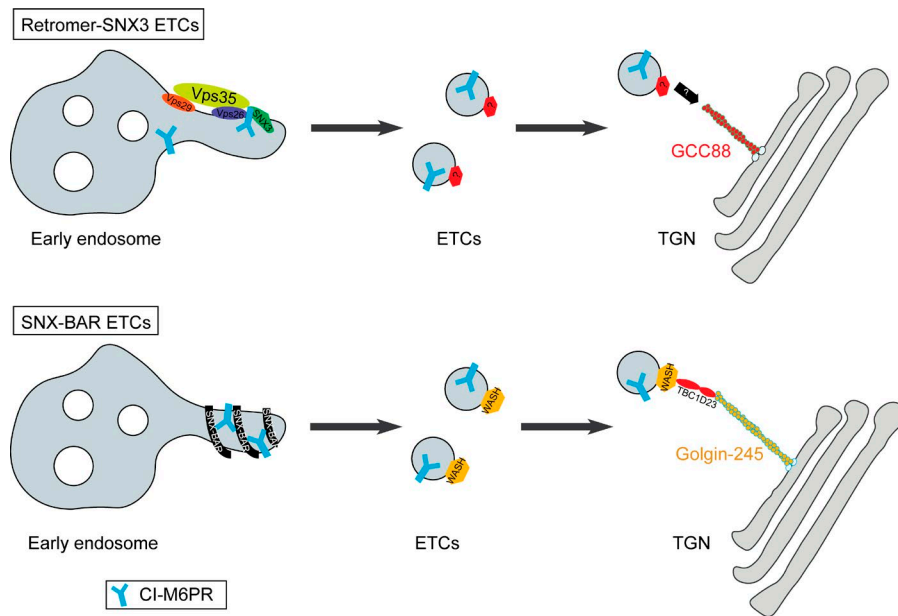
Figure 6. Evidence for two independent types of ETC responsible for the endosome-to-TGN transport of CI-M6PR in mammalian cells. In mammalian cells, CI-M6PR can be sorted into ETCs that depend on retromer/SNX3 and are tethered by GCC88 at the TGN. Alternatively, CI-M6PR can be sorted into ETCs that are independent of retromer but depend on SNX-BAR proteins and are tethered by golgin-245 at the TGN. The recently identified bridging protein TBC1D23 (Shin et al., 2017) is not required for tethering of the GCC88-dependent ETCs but is required for the tethering of ETC by golgin-245.

2017). However, we show that SNX27 is not required for the sorting and generation of retromer-mediated CI-M6PR ETCs. Hence, given that retromer function is restricted to CI-M6PR incorporation into ETCs tethered by GCC88, and that other endosomal proteins clearly also modulate CI-M6PR retrograde trafficking independent of the retromer, it is critical in future studies to determine how CI-M6PR is temporally and spatially organized on endosomes relative to these various proteins associated with distinct retrograde transport pathways.

Overall, we demonstrate the requirement of retromer in the retrograde trafficking of a subset of CI-M6PR–containing ETCs, which are defined by their capability to be tethered by the trans-golgin, GCC88. The sorting and generation of retromer-dependent CI-M6PR ETCs require SNX3, which is consistent with the structural features of the SNX3-retromer complex in cargo signal recognition and membrane recruitment (Lucas et al., 2016). Our working model is that the retromer is recruited to endosomal membranes through a direct interaction with SNX3 via its PI(3) P-binding PX domain (Harrison et al., 2014; Lucas et al., 2016; Priya et al., 2017; Lenoir et al., 2018). Although other regulators of retromer recruitment have been identified, including Rab7 (Rojas et al., 2008; Seaman et al., 2009) and SNX12 (Priya et al., 2017), a direct requirement for this retromer-dependent pathway needs to be determined given retromer's requirement to be distinctly spatially and temporally recruited for each of its multiple membrane transport pathways. Once recruited to the cargo-enriched endosomes, SNX3-retromer appears to selectively interact with the cytoplasmic domains of transmembrane cargoes including CI-M6PR. Retromer's direct role in the formation of ETCs is less clear, as we still observed the formation of GCC88-tethered ETCs which contain CD-M6PR in the absence of retromer. Retromer function may be restricted to the recruitment of cargo into the forming ETC, or alternatively, the ETC containing CD-M6PR observed are a distinct type of ETC that are also tethered by GCC88. After release from endosomes, the ETCs are recognized by tethering factors anchored at the TGN which capture the specific classes of

ETCs (Wong and Munro, 2014). The retromer-dependent subset of CI-M6PR ETCs are specifically recognized by GCC88, rather than golgin-97 or golgin-245. This specificity is consistent with observations that the tethering domains within golgin-97 and golgin-245 are related and quite different from that in GCC88 (Wong et al., 2017), and that the tethering of ETCs by GCC88 is independent of the bridging factor TBC1D23, which connects ETC-associated WASH with golgin-245 (Shin et al., 2017). We present a working model outlining the molecular evidence for at least two independent pathways for the formation and tethering of ETCs (Fig. 6). In conclusion, we have identified that retromer is involved in the sorting and generation of retrograde ETCs, and this pathway is critical for the efficient targeting of lysosomal enzymes, which contributes to the maintenance of lysosomal function.

Materials and methods
Chemicals, DNA constructs, and antibodies
Magic Red Cathepsin B Kit (938) was from ImmunoChemistry Technologies. DQ Red BSA (D12051) was purchased from Thermo Fisher Scientific. Cycloheximide (66-81-9) and AZD8055 (16978) were purchased from Cayman Chemical. Chloroquine (C6628) and Hepes (H3375-250G) were purchased from Sigma-Aldrich. TCA (T6399) was obtained from Sigma-Aldrich. 4-Methylumbelliferone (4-MU) standard (M333100) was obtained from Toronto Research Chemicals. 4-MU-acid phosphatase substrate (4-MU-phosphate; M8883), 4-MU-β-hexosaminidase substrate (4-MU-N-acetyl-β-glucosaminide; M2133), 4-MU-β-galactosidase substrate (4-MU-β-D-galactopyranoside; M1633) and 4-MU-β-glucocerebrosidase substrate (4-MU-β-glucopyranoside; M3633) were obtained from Sigma-Aldrich. Ponceau S solution (P7170) was purchased from Sigma-Aldrich. EDTA (180-500G) and sucrose (530-2KG) were from Univar. Protease inhibitor cocktail EDTA-free tablets (04 639 132 001) were obtained from Roche. Percoll (17-0891-01) was sourced from GE Healthcare. Glycine (010119.0500) was sourced from AnalaR.

Mitochondria-targeting golgins, including trans-golgins GC-C88ΔC-term-HA-monoamine oxidase A (MAO), golgin-97ΔC-term-HA-MAO, and golgin-245ΔC-term-HA-MAO, and cis-golgin GM130ΔC-term-HA-MAO, were obtained from S. Munro (Wong and Munro, 2014). The pCMU-CD8α-CI-M6PR construct was described previously (Lieu et al., 2007). The Vps35 CRISPR/Cas9 KO plasmid was purchased from Santa Cruz. The SNX3 CRISPR guide RNA (gRNA) plasmid (gRNA targeting sequence: 5′-CGGCCGACCCCCACCGTTTG-3′), SNX1 CRISPR gRNA plasmid (gRNA targeting sequence: 5′-AAATCATCCTACCATGTTAC-3′), and the SNX2 CRISPR gRNA plasmid (gRNA targeting sequence: 5′-TGATGGCATGAATGCCTATA-3′) were synthesized by Genscript. The pEGFP-N1-Vps35 plasmid has been described previously (Follett et al., 2014). To generate untagged WT Vps35 plasmid, full-length human Vps35 was amplified from the pEGFP-N1-Vps35 construct as a template using a 5′ primer (5′-CCCACCCGGTACCATGCCTACAACACAGCAG-3′) and a 3′ primer (5′-CCCACCCCTCGAGTTAAAGGATGAGACCTTCAT-3′) and subcloned into pcDNA3.1 (+) vector using KpnI and XhoI multicloning sites. The resulting construct was confirmed by DNA sequencing.

Mouse monoclonal anti–CI-M6PR (clone 2G11; ab2733), rabbit monoclonal anti–CI-M6PR (clone EPR6599; ab124767), mouse monoclonal anti-SNX27 (clone 1C6; ab77799), rabbit monoclonal anti–β-hexosaminidase/HEXB (clone EPR7978; ab140649), rabbit monoclonal anti–β-galactosidase-1 (clone EPR8250; ab128993), rabbit polyclonal anti–acid phosphatase 2 (ab84896), rabbit polyclonal anti–β-glucocerebrosidase/GBA antibody (ab92997), rabbit polyclonal anti-SNX3 (ab56078), rabbit polyclonal anti-LC3A/B (ab128025), and rabbit polyclonal anti-Vps26 (ab23892) were purchased from Abcam. Goat polyclonal anti-Vps35 (NB100-1397) was purchased from Novus Biologicals. Mouse monoclonal anti–CD-M6PR (22d4) was purchased from the Developmental Studies Hybridoma Bank. Mouse monoclonal anti-HA (clone 16B12; 901513) was purchased from BioLegend. Rabbit monoclonal anti-HA (clone C29F4; 3724), rabbit monoclonal anti–golgin-97 (clone D8P2K; 13192), rabbit monoclonal anti-Rab5 (clone C8B1; 3547), rabbit monoclonal anti–LC3B/LC3-II (clone D11; 3868), and rabbit monoclonal anti-mTOR (clone 7C10; 2983) were purchased from Cell Signaling Technology. Mouse monoclonal anti-CD8α (OKT8; 14-0086) was purchased from eBioscience. Mouse monoclonal anti-EEA1 (clone 14/EEA1; 610457), mouse monoclonal anti-p230 (clone 15/p230; 611280), and mouse monoclonal anti-LAMP1 (clone H4A3; 555798) were purchased from BD Biosciences. Mouse monoclonal anti-TfR (clone H68.4; 13-6800) was purchased from Life Technologies. Goat polyclonal anti–cathepsin-D (AF1014) was purchased from R&D Systems. Mouse monoclonal anti–α-tubulin (clone DM1A; T9026) and mouse monoclonal anti-GAPDH (clone GAPDH-71.1; G8795) were purchased from Sigma-Aldrich. Secondary donkey anti–mouse IgG Alexa Fluor 488 (A21202), donkey anti–mouse IgG Alexa Fluor 555 (A31570), donkey anti–rabbit IgG Alexa Fluor 488 (A21026), and donkey anti–rabbit IgG Alexa Fluor 555 (A31572) were purchased from Thermo Fisher Scientific.

Cell culture and transfection
HeLa cells (CCL-2; ATCC) were maintained in high-glucose DMEM (Thermo Fisher Scientific) supplemented with 10% FBS,

2 mM L-glutamine (Thermo Fisher Scientific), and 5 mg/ml penicillin and streptomycin (Thermo Fisher Scientific) in a humidified 37°C incubator with 5% CO_2. Transfection was performed using Lipofectamine 2000 (Thermo Fisher Scientific) according to manufacturer's instructions.

Generation of CRISPR/Cas9 KO cell lines
CRISPR/Cas9 KO cell lines were generated as previously described (Kerr et al., 2017). These cell lines were authenticated and confirmed to be mycoplasma free (CellBank Australia). Briefly, HeLa cells stably expressing mCherry-Cas9 were transiently transfected with the CRISPR gRNA plasmids targeting to Vps35, SNX1, SNX2, or SNX3 in a 60-mm dish. 48 h after transfection, cells were collected for FACS. GFP-positive cells were collected and allowed to grow until confluent. Cells were then diluted as 1 cell per well into 96-well plates until single colonies formed. CRISPR/Cas9-mediated knockout of targeted genes was confirmed by indirect immunofluorescence assay and immunoblot analysis. HeLa SNX1 KO cell line was transfected with CRISPR gRNA plasmid targeting to SNX2, and then subjected to the second round of single-cell sorting to generate SNX1/SNX2 dKO cell line. The SNX27 CRISPR/Cas9 KO cell line was previously generated (Clairfeuille et al., 2016).

Cell treatment procedure
For lysosomal degradation inhibition experiments, cells were treated with 50 μM chloroquine for 6 h; to inhibit mTORC1 activation, cells were treated with AZD8055, a mTORC1 inhibitor, for 25 h. To induce mTORC1 activation by essential amino acid, cells were starved in amino acid-free DMEM medium (D9800-13; USBiological) for 2 h before stimulated by MEM essential amino acid solution (final concentration: 2×; 11130051; Thermo Fisher Scientific) for 30 min.

Purification of lysosomal fractions
For lysosomal fraction purification, confluent cells were pelleted and resuspended in sucrose buffer (250 mM sucrose, 10 mM Hepes, and 1 mM EDTA, pH 7, supplemented with protease inhibitor cocktail). Cell lysates were homogenized and subjected to centrifugation at 1,000 rpm for 10 min at 4°C to separate the heavy membrane fraction (plasma and nuclear membranes) from the light membrane (endosomes, lysosomes, and ER, etc.) and cytosolic fractions. The light membrane and cytosolic fractions were then collected and layered onto an 18% (vol/vol) Percoll/sucrose buffer cushion and further subjected to centrifugation at 20,000 rpm for 1 h at 4°C. 16 fractions were collected and assayed for the activity of various lysosomal enzymes to confirm the enrichment of lysosomal vesicles.

Enzyme activity assay
The enzyme activity assay has been described previously (Leaback and Walker, 1961; Kolodny and Mumford, 1976). Briefly, each subcellular fraction was incubated with the respective 4-MU–linked substrate at 37°C for 30 min or 1 h. 4-MU–linked substrate only was used as a blank control. Reactions were stopped by 200 mM glycine buffer, and enzyme activity was assessed by fluorometric analysis (355/460 nm for 1.0 s) using the VICTOR[3] 1420 multilabel counter (PerkinElmer) and Wallac

1420 workstation software (PerkinElmer). The enzyme activity within each subfraction was normalized to input protein of the light membrane and cytosolic fraction.

Secretion assay

The secretion assay was performed as previously described (Follett et al., 2014). HeLa cells were seeded onto a 6-well plate 24 h before use. Cells were incubated with serum-free DMEM containing cycloheximide (100 µg/ml; Sigma-Aldrich) at 37°C for the indicated time points. Medium samples were collected, concentrated by using 10% TCA (Sigma-Aldrich) at 4°C overnight, and analyzed using Western blotting.

SDS-PAGE and Western immunoblotting

SDS-PAGE and Western blotting were performed as previously described (Yang et al., 2016). In brief, cell lysates were harvested in a lysis buffer containing protease inhibitor cocktail. Protein concentrations were quantified by Pierce bicinchoninic acid assay (Thermo Fisher Scientific). Equal amounts of protein samples were resolved on SDS-PAGE and transferred onto the PVDF membrane (Millipore) according to the manufacturer's instructions. Western blotting was developed either by enhanced chemiluminescent system using Clarity ECL substrate (Bio-Rad) or Odyssey infrared imaging system (LI-COR).

Internalization assay

HeLa cells grown on coverslips were cotransfected with the CD8α-M6PR reporter and individual mitochondria-targeting golgins for 24 h. Transfected cells were washed with ice-cold PBS twice and incubated in fresh serum-free medium containing anti-CD8α antibody (5 µg/ml) on ice for 30 min. After washing with ice-cold PBS and the low-pH solution containing 0.1 M glycine and 0.15 M NaCl, pH 3.0, to remove unbound antibodies, cells were then chased in serum-free medium for indicated time points at 37°C to allow the internalization of bound antibodies. At indicated time points, cells were fixed with 4% PFA and subjected to indirect immunofluorescence.

DQ Red BSA assay

HeLa cells grown on coverslips were incubated with culture medium containing 10 µg/ml DQ Red BSA (Thermo Fisher Scientific) at 37°C overnight. Cells were washed with PBS three times, fixed, and subjected to indirect immunofluorescence.

Magic Red Cathepsin-B assay

HeLa cells were seeded onto 96-well imaging plates at 30,000 cells per well 24 h before use. To measure lysosomal cathepsin B activity, cells were incubated with Magic Red Cathepsin-B Kit (ImmunoChemistry Technologies) according to the manufacturer's instructions, and live-cell time-lapse imaging was recorded using the Nikon Ti-E inverted microscope equipped with a 40× Plan Apochromatic objective.

Indirect immunofluorescence and colocalization analysis

Cells on coverslips were routinely fixed with 4% PFA in PBS for 15 min then permeabilized with 0.1% Triton X-100 in PBS for 10 min. Alternatively, for LC3 and mTORC1 staining, coverslips were fixed in ice-cold methanol for 5 min at −20°C. Fixed and permeabilized cell monolayers were blocked with 2% BSA in PBS for 30 min to reduce nonspecific binding. Cells were then labeled with diluted primary antibodies and corresponding secondary antibodies sequentially for 1 h at room temperature. Coverslips were mounted on glass microscope slides using Fluorescent Mounting Medium (Dako), and the images were taken at room temperature using the Zeiss LSM 710 Meta confocal laser scanning microscope or the Leica DMi8 SP8 Inverted confocal equipped with 63× Plan Apochromatic objectives. For quantification, images were taken from multiple random positions for each sample.

Images were processed using ImageJ software. Colocalization analysis was performed using the ImageJ *JACoP* plugin (Bolte and Cordelières, 2006). Transfected cells were segregated from fields of view containing both transfected and nontransfected cells by generating regions of interest. The selected region of interest was cropped, split into separated channels, and applied for threshold processing. Colocalization analysis was conducted on three independent experiments. Colocalization values were exported to GraphPad Prism 7 software and tabulated accordingly.

EM

EM was performed as previously described (Kerr et al., 2017). Briefly, cells seeded onto 35-mm dishes were fixed in 2.5% glutaraldehyde in PBS and processed for flat embedding in resin. Upon curing, the resin containing cells was broken away from the plastic dish. Ultrathin sections (60 nm) were cut and imaged using a Jeol 1011 transmission electron microscope at 80 kV fitted with a Morada Soft Imaging camera (Olympus) at twofold binning. The volume density of lysosomal compartments (defined by size and electron dense/multivesicular content) relative to the cytoplasmic volume was determined by point counting using a double lattice grid as described previously (Parton et al., 1989).

Statistics

All statistical analyses were completed using GraphPad Prism software 7 and described in the appropriate figure legends. Error bars on graphs were represented as ±SEM. P values were calculated using two-tailed Student's *t* test. P < 0.05 was considered significant.

Online supplemental material

Fig. S1 shows the full scan of the Western blot shown in Fig. 3 C and quantification data. Fig. S2 shows additional data for Figs. 4 and 5. Fig. S3 shows that the absence of retromer has no impact on the trafficking of CD-M6PR ETCs captured by golgin-97 or golgin-245. Fig. S4 shows that the retrograde transport of CI-M6PR ETCs captured by GCC88 and golgin-245 requires the coordination of SNX3 and SNX-BAR proteins, respectively. Fig. S5 shows that the retrograde transport of CD-M6PR ETCs captured by GCC88, golgin-97, or golgin-245 is not affected by the absence of SNX-BAR, SNX3, and SNX27 proteins.

Acknowledgments

References

Arighi, C.N., L.M. Hartnell, R.C. Aguilar, C.R. Haft, and J.S. Bonifacino. 2004. Role of the mammalian retromer in sorting of the cation-independent mannose 6-phosphate receptor. *J. Cell Biol.* 165:123–133. https://doi.org/10.1083/jcb.200312055

Arlt, H., F. Reggiori, and C. Ungermann. 2015. Retromer and the dynamin Vps1 cooperate in the retrieval of transmembrane proteins from vacuoles. *J. Cell Sci.* 128:645–655. https://doi.org/10.1242/jcs.132720

Bolte, S., and F.P. Cordelières. 2006. A guided tour into subcellular colocalization analysis in light microscopy. *J. Microsc.* 224:213–232. https://doi.org/10.1111/j.1365-2818.2006.01706.x

Breusegem, S.Y., and M.N.J. Seaman. 2014. Genome-wide RNAi screen reveals a role for multipass membrane proteins in endosome-to-golgi retrieval. *Cell Reports.* 9:1931–1945. https://doi.org/10.1016/j.celrep.2014.10.053

Bright, N.A., L.J. Davis, and J.P. Luzio. 2016. Endolysosomes Are the Principal Intracellular Sites of Acid Hydrolase Activity. *Curr. Biol.* 26:2233–2245. https://doi.org/10.1016/j.cub.2016.06.046

Bröcker, C., S. Engelbrecht-Vandré, and C. Ungermann. 2010. Multisubunit tethering complexes and their role in membrane fusion. *Curr. Biol.* 20:R943–R952. https://doi.org/10.1016/j.cub.2010.09.015

Bugarcic, A., Y. Zhe, M.C. Kerr, J. Griffin, B.M. Collins, and R.D. Teasdale. 2011. Vps26A and Vps26B subunits define distinct retromer complexes. *Traffic.* 12:1759–1773. https://doi.org/10.1111/j.1600-0854.2011.01284.x

Bulankina, A.V., A. Deggerich, D. Wenzel, K. Mutenda, J.G. Wittmann, M.G. Rudolph, K.N. Burger, and S. Höning. 2009. TIP47 functions in the biogenesis of lipid droplets. *J. Cell Biol.* 185:641–655. https://doi.org/10.1083/jcb.200812042

Carlton, J., M. Bujny, B.J. Peter, V.M. Oorschot, A. Rutherford, H. Mellor, J. Klumperman, H.T. McMahon, and P.J. Cullen. 2004. Sorting nexin-1 mediates tubular endosome-to-TGN transport through coincidence sensing of high- curvature membranes and 3-phosphoinositides. *Curr. Biol.* 14:1791–1800. https://doi.org/10.1016/j.cub.2004.09.077

Clairfeuille, T., C. Mas, A.S. Chan, Z. Yang, M. Tello-Lafoz, M. Chandra, J. Widagdo, M.C. Kerr, B. Paul, I. Mérida, et al. 2016. A molecular code for endosomal recycling of phosphorylated cargos by the SNX27-retromer complex. *Nat. Struct. Mol. Biol.* 23:921–932. https://doi.org/10.1038/nsmb.3290

Collins, B.M., S.J. Norwood, M.C. Kerr, D. Mahony, M.N. Seaman, R.D. Teasdale, and D.J. Owen. 2008. Structure of Vps26B and mapping of its interaction with the retromer protein complex. *Traffic.* 9:366–379. https://doi.org/10.1111/j.1600-0854.2007.00688.x

Díaz, E., and S.R. Pfeffer. 1998. TIP47: a cargo selection device for mannose 6-phosphate receptor trafficking. *Cell.* 93:433–443. https://doi.org/10.1016/S0092-8674(00)81171-X

Elwell, C.A., N. Czudnochowski, J. von Dollen, J.R. Johnson, R. Nakagawa, K. Mirrashidi, N.J. Krogan, J.N. Engel, and O.S. Rosenberg. 2017. *Chlamydia* interfere with an interaction between the mannose-6-phosphate receptor and sorting nexins to counteract host restriction. *eLife.* 6:e22709. https://doi.org/10.7554/eLife.22709

Follett, J., S.J. Norwood, N.A. Hamilton, M. Mohan, O. Kovtun, S. Tay, Y. Zhe, S.A. Wood, G.D. Mellick, P.A. Silburn, et al. 2014. The Vps35 D620N mutation linked to Parkinson's disease disrupts the cargo sorting function of retromer. *Traffic.* 15:230–244. https://doi.org/10.1111/tra.12136

Ghosh, P., N.M. Dahms, and S. Kornfeld. 2003. Mannose 6-phosphate receptors: new twists in the tale. *Nat. Rev. Mol. Cell Biol.* 4:202–212. https://doi.org/10.1038/nrm1050

Gillingham, A.K., and S. Munro. 2016. Finding the Golgi: Golgin Coiled-Coil Proteins Show the Way. *Trends Cell Biol.* 26:399–408. https://doi.org/10.1016/j.tcb.2016.02.005

Goberdhan, D.C., C. Wilson, and A.L. Harris. 2016. Amino Acid Sensing by mTORC1: Intracellular Transporters Mark the Spot. *Cell Metab.* 23:580–589. https://doi.org/10.1016/j.cmet.2016.03.013

Gokool, S., D. Tattersall, J.V. Reddy, and M.N. Seaman. 2007. Identification of a conserved motif required for Vps35p/Vps26p interaction and assembly of the retromer complex. *Biochem. J.* 408:287–295. https://doi.org/10.1042/BJ20070555

Gomez, T.S., and D.D. Billadeau. 2009. A FAM21-containing WASH complex regulates retromer-dependent sorting. *Dev. Cell.* 17:699–711. https://doi.org/10.1016/j.devcel.2009.09.009

Hara, S., E. Kiyokawa, S. Iemura, T. Natsume, T. Wassmer, P.J. Cullen, H. Hiai, and M. Matsuda. 2008. The DHR1 domain of DOCK180 binds to SNX5 and regulates cation-independent mannose 6-phosphate receptor transport. *Mol. Biol. Cell.* 19:3823–3835. https://doi.org/10.1091/mbc.e08-03-0314

Harbour, M.E., S.Y. Breusegem, R. Antrobus, C. Freeman, E. Reid, and M.N. Seaman. 2010. The cargo-selective retromer complex is a recruiting hub for protein complexes that regulate endosomal tubule dynamics. *J. Cell Sci.* 123:3703–3717. https://doi.org/10.1242/jcs.071472

Harbour, M.E., S.Y. Breusegem, and M.N. Seaman. 2012. Recruitment of the endosomal WASH complex is mediated by the extended 'tail' of Fam21 binding to the retromer protein Vps35. *Biochem. J.* 442:209–220. https://doi.org/10.1042/BJ20111761

Harrison, M.S., C.S. Hung, T.T. Liu, R. Christiano, T.C. Walther, and C.G. Burd. 2014. A mechanism for retromer endosomal coat complex assembly with cargo. *Proc. Natl. Acad. Sci. USA.* 111:267–272. https://doi.org/10.1073/pnas.1316482111

Harterink, M., F. Port, M.J. Lorenowicz, I.J. McGough, M. Silhankova, M.C. Betist, J.R.T. van Weering, R.G.H.P. van Heesbeen, T.C. Middelkoop, K. Basler, et al. 2011. A SNX3-dependent retromer pathway mediates retrograde transport of the Wnt sorting receptor Wntless and is required for Wnt secretion. *Nat. Cell Biol.* 13:914–923. https://doi.org/10.1038/ncb2281

Hierro, A., A.L. Rojas, R. Rojas, N. Murthy, G. Effantin, A.V. Kajava, A.C. Steven, J.S. Bonifacino, and J.H. Hurley. 2007. Functional architecture of the retromer cargo-recognition complex. *Nature.* 449:1063–1067. https://doi.org/10.1038/nature06216

Hirst, J., D.N. Itzhak, R. Antrobus, G.H.H. Borner, and M.S. Robinson. 2018. Role of the AP-5 adaptor protein complex in late endosome-to-Golgi retrieval. *PLoS Biol.* 16:e2004411. https://doi.org/10.1371/journal.pbio.2004411

Hong, Z., Y. Yang, C. Zhang, Y. Niu, K. Li, X. Zhao, and J.J. Liu. 2009. The retromer component SNX6 interacts with dynactin p150(Glued) and medi-

ates endosome-to-TGN transport. *Cell Res.* 19:1334–1349. https://doi.org/10.1038/cr.2009.130

Jia, D., T.S. Gomez, D.D. Billadeau, and M.K. Rosen. 2012. Multiple repeat elements within the FAM21 tail link the WASH actin regulatory complex to the retromer. *Mol. Biol. Cell.* 23:2352–2361. https://doi.org/10.1091/mbc.e11-12-1059

Kerr, M.C., J.S. Bennetts, F. Simpson, E.C. Thomas, C. Flegg, P.A. Gleeson, C. Wicking, and R.D. Teasdale. 2005. A novel mammalian retromer component, Vps26B. *Traffic.* 6:991–1001. https://doi.org/10.1111/j.1600-0854.2005.00328.x

Kerr, M.C., M.R. Lindsay, R. Luetterforst, N. Hamilton, F. Simpson, R.G. Parton, P.A. Gleeson, and R.D. Teasdale. 2006. Visualisation of macropinosome maturation by the recruitment of sorting nexins. *J. Cell Sci.* 119:3967–3980. https://doi.org/10.1242/jcs.03167

Kerr, M.C., G.A. Gomez, C. Ferguson, M.C. Tanzer, J.M. Murphy, A.S. Yap, R.G. Parton, W.M. Huston, and R.D. Teasdale. 2017. Laser-mediated rupture of chlamydial inclusions triggers pathogen egress and host cell necrosis. *Nat. Commun.* 8:14729. https://doi.org/10.1038/ncomms14729

Kingston, D., H. Chang, A. Ensser, H.R. Lee, J. Lee, S.H. Lee, J.U. Jung, and N.H. Cho. 2011. Inhibition of retromer activity by herpesvirus saimiri tip leads to CD4 downregulation and efficient T cell transformation. *J. Virol.* 85:10627–10638. https://doi.org/10.1128/JVI.00757-11

Kolodny, E.H., and R.A. Mumford. 1976. Human leukocyte acid hydrolases: characterization of eleven lysosomal enzymes and study of reaction conditions for their automated analysis. *Clin. Chim. Acta.* 70:247–257. https://doi.org/10.1016/0009-8981(76)90426-5

Kvainickas, A., A. Jimenez-Orgaz, H. Nägele, Z. Hu, J. Dengjel, and F. Steinberg. 2017. Cargo-selective SNX-BAR proteins mediate retromer trimer independent retrograde transport. *J. Cell Biol.* 216:3677–3693. https://doi.org/10.1083/jcb.201702137

Leaback, D.H., and P.G. Walker. 1961. Studies on glucosaminidase. 4. The fluorimetric assay of N-acetyl-beta-glucosaminidase. *Biochem. J.* 78:151–156. https://doi.org/10.1042/bj0780151

Lenoir, M., C. Ustunel, S. Rajesh, J. Kaur, D. Moreau, J. Gruenberg, and M. Overduin. 2018. Phosphorylation of conserved phosphoinositide binding pocket regulates sorting nexin membrane targeting. *Nat. Commun.* 9:993. https://doi.org/10.1038/s41467-018-03370-1

Lieu, Z.Z., and P.A. Gleeson. 2010. Identification of different itineraries and retromer components for endosome-to-Golgi transport of TGN38 and Shiga toxin. *Eur. J. Cell Biol.* 89:379–393. https://doi.org/10.1016/j.ejcb.2009.10.021

Lieu, Z.Z., M.C. Derby, R.D. Teasdale, C. Hart, P. Gunn, and P.A. Gleeson. 2007. The golgin GCC88 is required for efficient retrograde transport of cargo from the early endosomes to the trans-Golgi network. *Mol. Biol. Cell.* 18:4979–4991. https://doi.org/10.1091/mbc.e07-06-0622

Lucas, M., D.C. Gershlick, A. Vidaurrazaga, A.L. Rojas, J.S. Bonifacino, and A. Hierro. 2016. Structural mechanism for cargo recognition by the retromer complex. *Cell.* 167:1623–1635.e14. https://doi.org/10.1016/j.cell.2016.10.056

Markmann, S., M. Thelen, K. Cornils, M. Schweizer, N. Brocke-Ahmadinejad, T. Willnow, J. Heeren, V. Gieselmann, T. Braulke, and K. Kollmann. 2015. Lrp1/LDL Receptor Play Critical Roles in Mannose 6-Phosphate-Independent Lysosomal Enzyme Targeting. *Traffic.* 16:743–759. https://doi.org/10.1111/tra.12284

Maruzs, T., P. Lőrincz, Z. Szatmári, S. Széplaki, Z. Sándor, Z. Lakatos, G. Puska, G. Juhász, and M. Sass. 2015. Retromer Ensures the Degradation of Autophagic Cargo by Maintaining Lysosome Function in Drosophila. *Traffic.* 16:1088–1107. https://doi.org/10.1111/tra.12309

McGough, I.J., F. Steinberg, D. Jia, P.A. Barbuti, K.J. McMillan, K.J. Heesom, A.L. Whone, M.A. Caldwell, D.D. Billadeau, M.K. Rosen, and P.J. Cullen. 2014. Retromer binding to FAM21 and the WASH complex is perturbed by the Parkinson disease-linked VPS35(D620N) mutation. *Curr. Biol.* 24:1670–1676. https://doi.org/10.1016/j.cub.2014.06.024

McKenzie, J.E., B. Raisley, X. Zhou, N. Naslavsky, T. Taguchi, S. Caplan, and D. Sheff. 2012. Retromer guides STxB and CD8-M6PR from early to recycling endosomes, EHD1 guides STxB from recycling endosome to Golgi. *Traffic.* 13:1140–1159. https://doi.org/10.1111/j.1600-0854.2012.01374.x

Meyer, C., D. Zizioli, S. Lausmann, E.L. Eskelinen, J. Hamann, P. Saftig, K. von Figura, and P. Schu. 2000. mu1A-adaptin-deficient mice: lethality, loss of AP-1 binding and rerouting of mannose 6-phosphate receptors. *EMBO J.* 19:2193–2203. https://doi.org/10.1093/emboj/19.10.2193

Miura, E., T. Hasegawa, M. Konno, M. Suzuki, N. Sugeno, N. Fujikake, S. Geisler, M. Tabuchi, R. Oshima, A. Kikuchi, et al. 2014. VPS35 dysfunction impairs lysosomal degradation of α-synuclein and exacerbates neu-rotoxicity in a Drosophila model of Parkinson's disease. *Neurobiol. Dis.* 71:1–13. https://doi.org/10.1016/j.nbd.2014.07.014

Mizushima, N., T. Yoshimori, and B. Levine. 2010. Methods in mammalian autophagy research. *Cell.* 140:313–326. https://doi.org/10.1016/j.cell.2010.01.028

Munro, S. 2011. The golgin coiled-coil proteins of the Golgi apparatus. *Cold Spring Harb. Perspect. Biol.* 3:a005256. https://doi.org/10.1101/cshperspect.a005256

Osborne, D.G., C.A. Phillips-Krawczak, and D.D. Billadeau. 2015. Monitoring receptor trafficking following retromer and WASH deregulation. *Methods Cell Biol.* 130:199–213. https://doi.org/10.1016/bs.mcb.2015.03.018

Parton, R.G., K. Prydz, M. Bomsel, K. Simons, and G. Griffiths. 1989. Meeting of the apical and basolateral endocytic pathways of the Madin-Darby canine kidney cell in late endosomes. *J. Cell Biol.* 109:3259–3272. https://doi.org/10.1083/jcb.109.6.3259

Priya, A., J. Sugatha, S. Parveen, S. Lacas-Gervais, P. Raj, J. Gilleron, and S. Datta. 2017. Essential and selective role of SNX12 in transport of endocytic and retrograde cargo. *J. Cell Sci.* 130:2707–2721. https://doi.org/10.1242/jcs.201905

Rojas, R., T. van Vlijmen, G.A. Mardones, Y. Prabhu, A.L. Rojas, S. Mohammed, A.J. Heck, G. Raposo, P. van der Sluijs, and J.S. Bonifacino. 2008. Regulation of retromer recruitment to endosomes by sequential action of Rab5 and Rab7. *J. Cell Biol.* 183:513–526. https://doi.org/10.1083/jcb.200804048

Roy, S., A.M. Leidal, J. Ye, S.M. Ronen, and J. Debnath. 2017. Autophagy-dependent shuttling of TBC1D5 controls plasma membrane translocation of GLUT1 and glucose uptake. *Mol. Cell.* 67:84–95.e5. https://doi.org/10.1016/j.molcel.2017.05.020

Saftig, P., and J. Klumperman. 2009. Lysosome biogenesis and lysosomal membrane proteins: trafficking meets function. *Nat. Rev. Mol. Cell Biol.* 10:623–635. https://doi.org/10.1038/nrm2745

Saint-Pol, A., B. Yélamos, M. Amessou, I.G. Mills, M. Dugast, D. Tenza, P. Schu, C. Antony, H.T. McMahon, C. Lamaze, and L. Johannes. 2004. Clathrin adaptor epsinR is required for retrograde sorting on early endosomal membranes. *Dev. Cell.* 6:525–538. https://doi.org/10.1016/S1534-5807(04)00100-5

Scott, G.K., H. Fei, L. Thomas, G.R. Medigeshi, and G. Thomas. 2006. A PACS-1, GGA3 and CK2 complex regulates CI-MPR trafficking. *EMBO J.* 25:4423–4435. https://doi.org/10.1038/sj.emboj.7601336

Seaman, M.N. 2004. Cargo-selective endosomal sorting for retrieval to the Golgi requires retromer. *J. Cell Biol.* 165:111–122. https://doi.org/10.1083/jcb.200312034

Seaman, M.N. 2007. Identification of a novel conserved sorting motif required for retromer-mediated endosome-to-TGN retrieval. *J. Cell Sci.* 120:2378–2389. https://doi.org/10.1242/jcs.009654

Seaman, M.N. 2012. The retromer complex—endosomal protein recycling and beyond. *J. Cell Sci.* 125:4693–4702. https://doi.org/10.1242/jcs.103440

Seaman, M.N.J. 2018. Retromer and the cation-independent mannose 6-phosphate receptor-Time for a trial separation? *Traffic.* 19:150–152. https://doi.org/10.1111/tra.12542

Seaman, M.N., M.E. Harbour, D. Tattersall, E. Read, and N. Bright. 2009. Membrane recruitment of the cargo-selective retromer subcomplex is catalysed by the small GTPase Rab7 and inhibited by the Rab-GAP TBC1D5. *J. Cell Sci.* 122:2371–2382. https://doi.org/10.1242/jcs.048686

Settembre, C., A. Fraldi, D.L. Medina, and A. Ballabio. 2013. Signals from the lysosome: a control centre for cellular clearance and energy metabolism. *Nat. Rev. Mol. Cell Biol.* 14:283–296. https://doi.org/10.1038/nrm3565

Shin, J.J.H., A.K. Gillingham, F. Begum, J. Chadwick, and S. Munro. 2017. TBC1D23 is a bridging factor for endosomal vesicle capture by golgins at the trans-Golgi. *Nat. Cell Biol.* 19:1424–1432. https://doi.org/10.1038/ncb3627

Simonetti, B., C.M. Danson, K.J. Heesom, and P.J. Cullen. 2017. Sequence-dependent cargo recognition by SNX-BARs mediates retromer-independent transport of CI-MPR. *J. Cell Biol.* 216:3695–3712. https://doi.org/10.1083/jcb.201703015

Tabuchi, M., I. Yanatori, Y. Kawai, and F. Kishi. 2010. Retromer-mediated direct sorting is required for proper endosomal recycling of the mammalian iron transporter DMT1. *J. Cell Sci.* 123:756–766. https://doi.org/10.1242/jcs.060574

Tammineni, P., Y.Y. Jeong, T. Feng, D. Aikal, and Q. Cai. 2017. Impaired axonal retrograde trafficking of the retromer complex augments lysosomal deficits in Alzheimer's disease neurons. *Hum. Mol. Genet.* 26:4352–4366. https://doi.org/10.1093/hmg/ddx321

Vardarajan, B.N., S.Y. Bruesegem, M.E. Harbour, R. Inzelberg, R. Friedland, P. St George-Hyslop, M.N. Seaman, and L.A. Farrer. 2012. Identification of

Alzheimer disease-associated variants in genes that regulate retromer function. *Neurobiol. Aging.* 33:e2215–e2230. https://doi.org/10.1016/j.neurobiolaging.2012.04.020

Wang, S., K.L. Tan, M.A. Agosto, B. Xiong, S. Yamamoto, H. Sandoval, M. Jaiswal, V. Bayat, K. Zhang, W.L. Charng, et al. 2014. The retromer complex is required for rhodopsin recycling and its loss leads to photoreceptor degeneration. *PLoS Biol.* 12:e1001847. https://doi.org/10.1371/journal.pbio.1001847

Wassmer, T., N. Attar, M.V. Bujny, J. Oakley, C.J. Traer, and P.J. Cullen. 2007. A loss-of-function screen reveals SNX5 and SNX6 as potential components of the mammalian retromer. *J. Cell Sci.* 120:45–54. https://doi.org/10.1242/jcs.03302

Wong, M., and S. Munro. 2014. Membrane trafficking. The specificity of vesicle traffic to the Golgi is encoded in the golgin coiled-coil proteins. *Science.* 346:1256898. https://doi.org/10.1126/science.1256898

Wong, M., A.K. Gillingham, and S. Munro. 2017. The golgin coiled-coil proteins capture different types of transport carriers via distinct N-terminal motifs. *BMC Biol.* 15:3. https://doi.org/10.1186/s12915-016-0345-3

Yang, Z., L.K. Hong, J. Follett, M. Wabitsch, N.A. Hamilton, B.M. Collins, A. Bugarcic, and R.D. Teasdale. 2016. Functional characterization of retromer in GLUT4 storage vesicle formation and adipocyte differentiation. *FASEB J.* 30:1037–1050. https://doi.org/10.1096/fj.15-274704